MECHANISMS GOVERNING ONSET OF SLIDING FRICTION

By

VIJAY KRISHNAN SUBRAMANIAN

Bachelor of Engineering in Mechanical
Anna University
Chennai, Tamil Nadu, India
2005

Master of Science in Mechanical
Oklahoma State University
Stillwater, Oklahoma, USA
2010

Submitted to the Faculty of the
Graduate College of
Oklahoma State University
in partial fulfillment of
the requirements for
the Degree of
DOCTOR OF PHILOSOPHY
DECEMBER, 2014

MECHANISMS GOVERNING ONSET OF SLIDING FRICTION

Thesis Approved:

Dr. Raman P. Singh, Dissertation Adviser

Dr. Kaan Kalkan

Dr. Sandip P. Harimkar

Dr. Ranji Vaidyanathan

ACKNOWLEDGMENTS

I convey my sincere gratitude to the following people for their role in my successful completion of my dissertation. Along these years, they have not only played an active role in my research but also influenced the development of my professional and personal attitude.

My dissertation chair and advisor, Dr. Raman P. Singh, for rekindling and supporting my research on frictional sliding.

My committee members, Dr. Kaan Kalkan, Dr. Ranji Vaidyanathan, Dr. Sandip Harimkar, and Dr. Xiaoliang Jin for their constructive suggestions and interpretations of my friction research.

Dr. Demir Coker, currently at METU (Ankara, Turkey) for introducing me to this field of sliding friction.

My former advisor, Dr. Hongbing Lu (currently at Univeristy of Texas at Dallas), for training me in experimental solid mechanics. His 2D-DIC program has been used to batch process high-speed camera data in this dissertation.

MAML (current and previous) lab members, including Dr. Arif Rahman, Salah U. Hamim, Dr. Suraj Zunjarrao, Dr. Abhishek Singh, Dr. Gajendra Pandey, and other colleagues for sustaining the conducive and collaborative research ambiance in the group.

My parents and sibling, Revathy, for their continued motivation and patience.

My wife, Sharanya, for being my strongest believer, supporter, and critic.

Acknowledgements reflect the views of the author and are not endorsed by committee members or Oklahoma State University.

Name: Vijay Krishnan Subramanian

Date of Degree: DECEMBER, 2014

Title of Study: MECHANISMS GOVERNING ONSET OF SLIDING FRICTION

Major Field: Mechanical Engineering

Abstract: Experimental observations on slip onset during quasistatic shearing of bimaterial interface are presented in this study. Although friction has been a subject of multi-disciplinary research for many decades, events surrounding the transition of static to dynamic friction are not well understood. In this fundamental study of dry frictional sliding in polyurethane (PU)–poly(methyl methacrylate) (PMMA) material pair, we provide experimental evidences on propagation of slow rupture waves prior to slip onset. Constant normal load of 114 N and sliding velocity of 0.4 mm/s were chosen to induce stick-slip oscillations in the PU-PMMA sliding pair. Full-field, non-invasive techniques of dynamic photoelasticity and 2D Digital Image Correlation (2D DIC) were used simultaneously to capture and analyze the propagation of rupture fronts from the leading to trailing edges. Sequence of 900 images before and after onset of slip were acquired using high-speed photography at 44,000 frames/s. Analysis of grey-scale speckles using DIC, provided information on magnitude, direction, and velocity of slip. Based on the wave and particle data, we conclude that slower sub-shear waves produced the onset of slip. Velocity of sub–shear front was found to be around 30-85 m/s, while instantaneous slip velocities reached maximum values of 0.3 m/s. Origin of these rupture fronts was traced to a point near the tip of the leading edge in PU. Our experiments clearly demonstrate the role of characteristic waves along the interface during sliding friction.

TABLE OF CONTENTS

LIST OF TABLES

LIST OF FIGURES

CHAPTER 1

INTRODUCTION

Friction is the phenomenon of resistance to relative motion between two bodies. It is existent in multiple length scales from nano– to geo– scale. We experience positive and negative effects of friction in our everyday lives. Friction provides traction while walking, driving and braking vehicles, prevents mountains and buildings from crumbling into dirt, and plays critical role in simple tasks such as writing and chewing. Friction is also a leading cause of waste or inefficiency in our society. It leads to wear and/or heat generation between two surfaces in relative motion such as in bearings, motors, gears, and internal combustion engines. Since early days, man has tried to manipulate friction to his benefit. Rubbing of stones to produce fire is one of the first discoveries by human beings utilizing friction. Use of sledges and wheels for transporting goods have been discovered as early as 3000 BC. Although, human beings have tackled friction, it was not until the start of 19^{th} century that a scientific approach to measuring and reducing friction was instituted and called as tribology. Since then numerous techniques for understanding and measuring frictional dissipation, lubrication, and wear have been developed.

Tribology, more specifically friction, is a multi-disciplinary field of study not limited to physics, solid mechanics, material science, engineering, geology, and medicine (prosthetics). It is a surface phenomenon often studied in conjunction with adhesion and surface roughness. The presence of third body between the sliding interface such as fluid film is known to drastically alter the interfacial friction behavior. In this thesis, I focus my research on fundamental understanding of physical processes leading to onset of dry (without lubrication) frictional sliding using experiments. Using a simple two-body sliding setup, the onset of sliding is observed in microsecond time scale and analyzed using different experimental techniques. Observations and results documented in the later chapters of this dissertation clearly demonstrate the role of rupture propagations during sliding onset. Quantitative data on frictional sliding characteristics have also been presented in detail. The results generated in the course of this study shall serve as input for modeling frictional sliding behavior.

Chapter 2 summarizes the review of previous experimental and numerical modeling work reported in literature on dry frictional sliding systems. A chronological sequence of key developments in friction research is presented. Many improvements in modeling frictional sliding behavior have come about in the last two decades, aided by advancements in experimental capabilities to resolve sliding event in time and space. Recent experimental studies highlighting the role of rupture waves in sliding onset are discussed. Different modes of sliding have been postulated but experimental verification is still required. Such modes are discussed and their differences have been highlighted. After the review of existing literature, some

unanswered questions on frictional sliding onset have been identified and discussed. Based on this, I have developed my research motivation and questions that I aim to answer in this dissertation.

In Chapter 3, a detailed documentation of experimental methodologies used in this study is provided. Other details such as specimen preparation and their properties have also been documented with the aim of facilitating replication of my lab scale frictional sliding experiments elsewhere. This study focuses on the sliding pair of polyurethane–Plexiglas due to favorable properties of these polymers such as refringence, slow wave speeds in polyurethane, and wave speed mismatch at the bimaterial interface. We believe that the results are more general and not confined to the polymer blocks tested here. A recipe for further experimental tests has been identified, which when applied to other material pairs along with suitable high-speed cameras, appropriate framing rates, and frame counts can provide details on the onset of sliding in sliding pairs.

Experimental evidence on existence of rupture waves, along the interface during sliding onset at slow slider speeds, is presented in Chapter 4. Results from high-speed camera observations clearly demonstrate the precursors leading to onset of slip in polyurethane–Plexiglas interface. Photoelastic fringe data show propagation of various rupture fronts along the interface before sliding initiation. We not only report the existence of such unique wave fronts, but also map particle deformations close to the sliding interface as the rupture fronts propagate. Although numerous researchers have reported the overall frictional properties, we show the localized

nature of friction and the crack-like propagation of rupture waves along the interface during sliding. Analysis of the photoelastic fringes, provided an estimate of local friction coefficient leading to onset of sliding and the variations in friction coefficient during slip. Effects of loading parameters namely, normal load and slider velocity have been investigated and presented. Evidence of rupture front origin along the interface is presented as well. Source of sliding pulses are modified by introducing a thin, low friction tape made of Teflon in middle of the sliding interface. The reduced resistance to shear along this weak interface, emitted slip pulses prior to sliding.

Chapter 5 concludes the findings of this study along with suggestions for further work.

CHAPTER 2

Review of Existing Literature

This section reviews the key findings and progress reported in literature.

2.1 Timeline of Key Developments in Friction

Leonardo da Vinci (around 1500 AD) is credited with the first scientific study of friction. His experiments on sliding of objects along inclined planes and onset of sliding using suspended mass lead to the first friction law. Through his experiments two key observations arose: (a) friction was independent of area of contact, and (b) the force needed to pull an object was dependent on the normal force exerted on the body. These two observations form the basis of simple empirical friction law proposed by him; the ratio of pull force (F_S) to normal force (F_n) is equal to the term called as coefficient of friction, or $\mu = \frac{F_S}{F_n}$. He found the value of μ to be 0.25 for most material pairs, thereby called it universal friction coefficient.

In 1699 , Guillaume Amontons independently reported the proportionality of normal and friction loads. He found 0.33 to the material independent friction

coefficient. Further improvements to Amontons' friction law were made by Charles Augustin de Coulomb in 1785. Coulomb believed that friction coefficient was independent of sliding velocity for a sufficiently long period of sliding. He also found the friction coefficient to reach a peak value (μ_s) just before the object started sliding and dropped to a constant value during continuous sliding (μ_d), as shown in figure 2.2. He thus came up the static and dynamic friction regimes.

$$\mu_s \geq \mu_d$$

Another important contribution of Coulomb is the influence of adhesion in frictional behavior. He suggested that friction is made of two terms, one from the normal loading (Amontons' law), and the other from adhesion. The adhesion term was ignored as it was found to be insignificant for the large scale of objects that he tested. With the recent advent of precision atomic force probes, adhesion has been found to play a major role at small (nanometer) length scales. Amontons-Coulomb friction law still prevails and is widely used, particularly in engineering and contact problems due to their simplicity. Unlike Newton's laws of motion, Amontons-Coulomb friction law does not explain the fundamental nature of friction. The law does not take into account various complex mechanical, thermal, plastic, and chemical processes occuring at material interfaces. Amontons estimated friction coefficient to be independent of sliding area. Recent studies have been able to estimate the actual area of contact to be around 1% of nomical contact area [33].

In 1950, Philip Bowden and David Tabor [13] investigated the physical cause for

friction. For their extensive studies on friction, they are rightly referred to modern pioneers of tribology (study of friction). Most notable amongst their contributions are the experimental measurement of real area of contact between two surfaces. One such method was the use of electrical resistivity between two metallic surfaces. They found a linear dependence of friction coefficient to the actual area of contact. Instead of the previously held notion that friction arises primarily from interlocking of asperities, they found that adhesion and shear strength of the asperities at the junction to play a dominant role in frictional sliding behavior. However, recent tests show that adhesion is significant only at nano length scales.

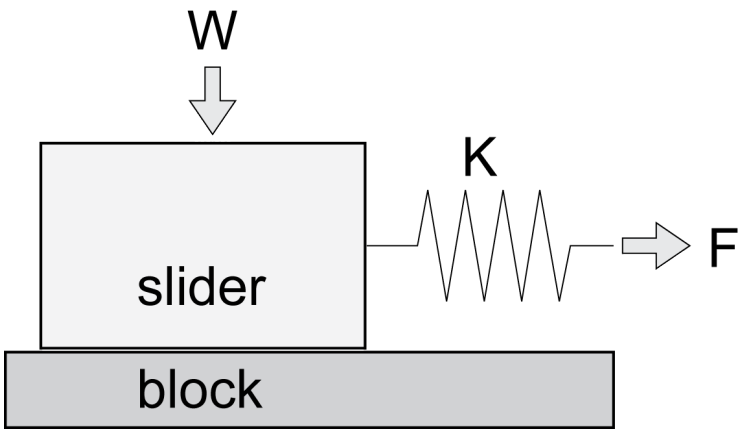

Figure 2.1: Schematic of block and slider system. The slider is pressed on the stationary block by a normal force 'W'. The slider is pulled by a tangential force 'F' and stiffness 'K'.

Although frictional sliding coefficient was thought to be constant upon the onset of sliding, researchers have observed various frictional oscillations during sliding in their lab experiments. These unsteady sliding regimes are broadly called as stick-slip, as illustrated in figure 2.2. Stick-slip has been widely researched in friction

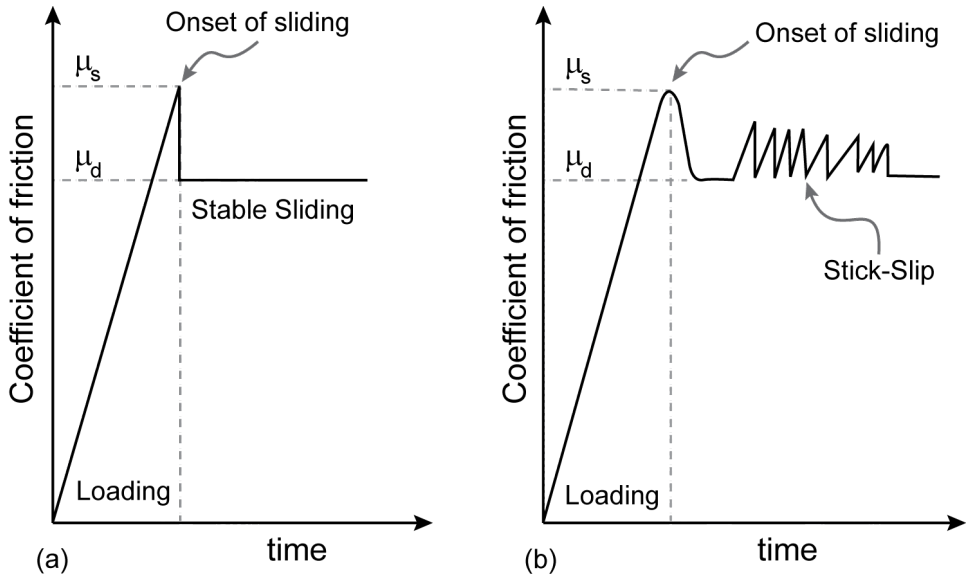

Figure 2.2: (a) Schematic of variation of friction coefficient with time as predicted by Amontons-Coulomb law. Sliding begins when the friction coefficient reaches a critical value, μ_s, and then drops to a constant value of μ_d, (b) Stick-slip or unsteady sliding observed in sliding friction experiments when sliding velocity changes. .

for the past fifty years, with the primary motivation of identifying the conditions under which stick-slip can be avoided. In most practical applications stick-slip is generally avoided, such as squealing in the brakes, screeching of tires, formation of discontinuous chips in metal cutting operations, and widely unpopular squeal of chalk on blackboard.

The long-held assumption of friction coefficient being independent of sliding velocity now needed to be changed. In a physical study of stick-slip by Rabinowicz [29], in 1958, suggested that kinetic friction was dependent on the sliding history. Using the classical block and slider system, shown in figure 2.1, he proposed memory effect in sliding friction which lead to a lag in friction sliding

Figure 2.3: Photograph of a fence offset by 2.6 m (8.5 ft) during 8.2 magnitude earthquake on April 18, 1906 at San Fransisco, California. This picture illustrates the lateral (shear) movement of the San Andreas fault. Photograph provided for free use by NOAA/NGDC, G.K. Gilbert, U.S. Geological Survey.

response when the tangential (pull) velocity was changed instantaneously. He deduced the existence of a lower limit in critical slip distance, around 10^{-3} cm, before which stick-slip would not occur.

2.2 Implications of Frictional Sliding Onset

Unlike numerous studies on various aspects of friction and wear, including measurements of static and dynamic friction coefficients, study of onset and modes of sliding is still a fundamental problem of multiple length scales. In this section,

the various areas benefiting from this study of frictional sliding are discussed.

2.2.1 Friction and Earthquakes

Brace and Byerlee [14, 15], in 1966, introduced the idea of earthquakes resembling stick-slip. The slip phase is the event of catastrophic fault sliding (earthquake tremor) and the stick phase is the long period of load build-up. The slip phase lasts a few seconds whereas the stick phase could last up to few centuries. One important question highlighted in their work is the extent of stress drop in lab experiments versus that observed in earthquakes. In their lab experiments, they observed drop in stresses to be drastic during slip phase, whereas a gradual stress drop was observed during earthquakes. This raises the important question on how to relate laboratory experiments to real-life observations. Seismology triggered major interest in the scientific community to investigate the underlying phenomenon of friction. Figure 2.3 shows a photograph of neat shear offset during 1906 San Fransisco earthquake, where the fence was sheared by a distance of about 8 feet. Following Rabinowicz's idea of sliding history affecting dynamic friction, the rate and state friction (RSF) law was introduced later by Dieterich and Ruina. Implementation of RSF law in predicting lab-scale earthquakes in rocks has been demonstrated. However the use of RSF law in predicting slips in tectonic plates is still an area of active research [7]. Mimicking the physical behavior of earthquakes in lab scale has been complicated by length and time -scale effects, suitable material representation of sliding pairs, and complications in visualizing the stress state along the faults. Small scale deformations along the fault zones are poorly understood and are still a

subject of intense investigation.

2.2.2 Friction in Fiber Matrix Composites - A Toughening Mechanism

Tsai and Kim [39] conducted pull-out tests on glass fiber embedded in epoxy matrix. The response of the fiber-matrix system was characterized at different velocities of pull-out. Using load measurements in conjunction with photoelasticity, they were able to study the fiber debonding process in detail. The glass fibers, instead of rods, of diameter 200 μm and average surface roughness of 1.2 Å were embedded in quick-setting epoxy. The fibers were coated either with acrylate or gold-palladium coating, in order to modify the bonding strength between fiber and matrix. The fibers were then pulled at constant rate of displacement. While stick-slip was observed in all the tests, the pull-out processes were different. Photoelastic images showed evolution of fringes in the fiber-matrix interface which grew in size prior to debonding event. They described this debonding to be interfacial crack propagation although there were no detailed investigation. The camera used to monitor the photoelastic fringes was also a regular TV camera with low framing rate of 30 fps. So not much is known on the nature of crack propagation from this study. After the crack-like event on the leading edge, the fiber then pulled in two ways; either by partial sliding or full sliding depending on the coating and the velocity. For the acrylate coating, after the initial debonding phase, partial sliding with stick-slip was observed. In the case of Au-Pa coating, after initial debonding, the entire surface was seen to be sliding with little to no stick-slip. This important study has motivated further interest in to knowing the origins of events at the sliding interface that govern the nature of sliding.

2.2.3 Friction in Tires

Friction in rubber is not limited to tires but also to windshield wipers, shoes, seals, rollers, and winding mechanisms. The need for an accurate friction model is critical to predicting sliding behavior under different loads, velocities, and temperatures. Apart from choice of rubber material, patterns or grooves on the surface have been found to influence the sliding behavior under dry and wet conditions. Recently studies have focused on effect of micro patterns on the surface of rubber to alter sliding friction behavior [26]. Sliding tests on patterned rubber – smooth glass plate conducted by Audry et al. [3] found crack-like sliding behavior and surface patterns effected the crack initiation stresses. Contact mechanics studies on rubber friction on smooth and rough surfaces by Persson [27, 28] show that the effect of length-scale variations in surface roughness to follow a simple relationship, $v/\lambda \approx 1/\tau$, where v is the sliding velocity, λ is the wavelength of surface roughness, and τ is the relaxation time of rubber. This means that the contributions of different wavelengths of surface roughness become prominent at different sliding velocities. An accurate multi-scale friction model is still a challenge which emphasizes the need for fundamental understanding of sliding friction behavior.

2.3 Rate and State Friction (RSF) Law

In 1979, Dieterich [18] published the results of his experiments on evolution of instabilities in rock materials which improvised on Rabinowicz's memory effect of

friction. From his experiments, he found that friction was not only dependent on the instantaneous velocity of slider, also called the rate variable. The rate variable arises from the velocity-weakening characteristic of sliding friction. This means that when the velocity of the slider increases, there is a decrease in the frictional resistance, thereby leading to a further increase in acceleration. The opposite trend is observed when the slider velocity is decreased. Dieterich showed that the transient duration exhibited by the system can be expressed as $\Delta t \approx D_0/V_f$, where D_0 is the characteristic length, usually in micrometers (determined experimentally).

Frictional interface strengthening with aging, i.e. at rest the frictional interface becomes stronger as time increases. Upon sliding intiation, dynamic aging decreases with increasing sliding velocity, which indicates the evolution of the physical state with time. Based on the experiments by Dieterich, Ruina [36] and Rice and Ruina [31] formulated the rate and state friction law, given in equations (2.1) and (2.2).

$$\mu = \frac{F}{N} = \mu_d(V_0) + A \ln\left(\frac{\dot{x}}{V_0}\right) + B \ln\left(\frac{\phi V_0}{D_0}\right) \tag{2.1}$$

$$\dot{\phi} = 1 - \frac{\dot{x}\phi}{D_0} \tag{2.2}$$

where, F is the shear force, N is the normal force, V_0 is the initial sliding velocity, D_0 is the characteristic sliding distance, ϕ is average time spent by the micro-contacts at the interface being in rest. When the interface is in motion, the micro-contact configurations are destroyed after a finite sliding distance. In this case, the average time of contact is given by $\phi = D_0/V$, which is interrupted by motion. One of

the biggest consequences of the rate and state friction law is the variable nature of dynamic friction coefficient (μ_d) which was previously thought to be constant for a given material pair. Now, μ_d is not only dependent on the instantaneous change in velocity, but also on the previous dynamical history of the contact. Recently, Coker et al. simulated various sliding modes using rate and state friction model for cases of high-velocity impact of projectile along the bimaterial interface [16].

2.3.1 Static Aging - Variable Nature of Static Friction

Experimental observations from stop-and-go tests reveal time dependence of static friction coefficient at interfaces of various materials. As the time of stationary contact increased, the static friction threshold was also found to increase. This leads to the question if the value of μ_s is indeed constant for a material pair? Dieterich (1972) [17] showed that static friction increases approximately with logarithmic increase in holding time for rocks. Slopes of aging curves for various materials have been found to be in the order of 10^{-2}. Creep growth model explained this time dependence on static friction. Berthoud [12] conducted temperature based aging tests to confirm creep like mechanism in PMMA. Viscoelastic creep behavior was observed in rubber aging on glass surfaces by Persson [28]. This phenomenon of static aging is also called pinning. Pinning has also been observed in earth quake faults. It is also interesting to know that soft gelatin gels show similar aging behavior in glass, as demonstrated by Baumberger et al. [6]. They conducted sliding friction tests of gels on glass surface in the absence of normal loads. The friction behavior in the case was found to be dominated by development of adhesive contact between

the gel-glass interface. Baumberger and Caroli [5] suggested the classification of dry sliding interfaces in to two classes; (a) Rough, hard solids, and (b) Soft, smooth solids. Rough, hard solid (with high elastic modulus) interfaces under "reasonably" high loads do not have atomic level contacts between the surfaces and are instead dominated by micro-contacts which constitute the actual area of contact. Hence the micrometer length scale becomes relevant. Whereas, soft smooth solid interfaces have intimate contact throughout the surface, thereby making nanometric length scales relevant. Such a classification prevented the need to categorize interfaces based on length scales.

2.4 Friction – How Sliding Initiates?

Investigations of events surrounding the detachment process prior to sliding have primarily taken place at two research groups; Fineberg's group at Israel and Rosakis' group at USA.

Fineberg et al. [9, 32, 35] measured the real area of contact using the technique of total internal reflection, as seen in figure. A laser beam passed through the interface of PMMA on PMMA, at an angle such that the beam undergoes reflection at the air gaps between the micro-contacts while transmission occurs at the points of contact. A fast framing camera was used to acquire the transmitted beam, thereby measuring the areas of contact in real-time. Using this data coupled with the normal and shear loads for different sliding velocities (driven by a stepper motor), the onset of sliding was investigated. Static tests done to measure change in contact area with normal

loading, showed linear relationship. This matched with previous observations of Dieterich and Kilgore [19]. When shear is imposed on the slider, rapid processes were detected prior to sliding. Photographs of contact area provide the details of the dynamics at the interface. Prior to the onset of sliding, a sub-Raleigh (0.4-0.5V_R) crack-like wave front propagates from the trailing towards the interface. Once the front reaches close to the Raleigh wave speed, the front splits in to two parts, intersonic (1.3-1.8V_R), and slow front.

This phenomenon of wave bifurcation appears similar to that observed by Lykotrafitis and Rosakis [24] in their dynamic shear loading experiments along the bimaterial interface of plexiglas on steel. In both these studies, the role of intersonic fronts on the interface is not clear. On the other hand, the slow wave fronts seem to correlate with significant reduction in contact area. These slow fronts were found to either propagate through the interface or reverse in to sub-Raleigh fronts. Upon the arrival of the slow or sub-Raleigh front at the leading edge, sliding initiates. With continued application of shear, the three wavefronts are repeatedly created and resultant sliding is stick-slip.

2.4.1 Rupture Sliding Mode: Shear Crack-like or Pulse-like?

One of the lingering questions in the field of friction is the nature of detachment process. Currently, two accepted modes of sliding are the crack-like and pulse-like sliding modes. These two modes differ by the amount of slip along the interface as compared to the sliding across the entire surface. In the crack-like sliding mode, the

surfaces behind the crack tip continue sliding after the passage of the rupture front. In the case of pulse-like sliding, sliding occurs over relatively localized regions followed by interlocking of surface. Crack-like model is the currently accepted mode of frictional sliding [44]. Propagation of rupture along the interface is modeled as shear wave propagation in Mode-II fracture. In 1990, Heaton reported seismic inversion data collected from earthquakes, which showed that the duration of slip to be one order of magnitude slower than the entire slip duration [21]. The amount of frictional heat generation was found to be lower than predicted by the shear crack model. Slip pulses were reported in the experiments conducted by Anooshehpoor [2], in their lab tests on dissimilar rubber foams. Pulse-like sliding modes have also been observed in the simulations and experiments of Rosakis et al. [16, 24]. A high-speed projectile impact on homogeneous and bimaterial interfaces, initiated sliding along the interface. Pulse-like rupture modes were observed in cases of high normal stresses and low impact velocities only in monolithic material pair of homalite on homalite. For the bimaterial cases, no pulse-like modes were observed. Rupture fronts in the order or shear and Rayleigh wave speeds were found to be preceding the slip event.

Schallamach Waves

In sliding interfaces of rubber on rigid surfaces, Schallamach observed a unique mechanism of sliding where waves of detachment propagated on rubber surface. These ripple–like fronts propagate against the direction of prescribed shear [4, 37]. These waves resemble the ripple–like motion in carpets, where no true sliding occurs.

Apparent sliding is a result of propagation of the folds/ripples across the interface. These waves are called as Schallamach waves. Velocity of these detachment waves has been found to be dependent on imposed sliding velocity. Schallamach waves can be identified by (i) decrease in contact area during the propagation of the ripple front, and (ii) the detachment wave velocity is in the order of 1–10 mm/s [20].

Weertman Pulses

Wrinkle-like pulses were predicted in bimaterials due to differences in wave speeds across the interface [41, 42]. These pulses are called as Weertman pulses, and propagate across the interface between $v_{Rayleigh}$ and v_{shear} of the slower medium. Opening pulse is produced from the difference in wave speeds along perpendicular and parallel directions of the interface. Experimental observations of wrinkle-like pulses in dissimilar material interfaces have been reported [1, 2, 24].

2.4.2 Conclusion of Literature review

Friction is a widely studied by researchers in various disciplines, however our knowledge on conditions leading to onset of frictional sliding are still limited. Amontons-Coloumb friction law has been widely adopted due to its simplicity and applicability. Research in friction laws lead to development of phenomenological models such rate and state friction law and its iterations. These rate and state models developed from experimental studies. Numerous studies focused on characterizing frictional sliding behavior based on measurement of global values of normal

and shear stresses. Parameters such as sliding speeds and third phase along the interface were varied and their effects on friction coefficient were measured. However, fundamental theory of sliding friction has proved to be elusive and is still difficult [40]. Recent advances in technological capabilities as well as developments in seismic measurements, lead to an increased interest in study of frictional sliding event in microscale time resolution.

Unlike fracture, it is still not possible to predict the onset of sliding reliably even in lab scale models. This also explains the reason why earthquakes cannot be accurately predicted. While fracture toughness is material property, there is no such quantity discovered in relation to friction. Laboratory tests on sliding between material pairs have shown varying values of static friction coefficient [10, 30]. The traditionally held notion of μ_s being constant for a given material pair, has come under question. These experimental studies show that μ_s ($= \frac{\sigma_s}{\sigma_n}$), at localized region near the interface, prior to slip reach values that are many times higher than the globally obtained μ_s from the load cell data. Experiments conducted by Ben-David and Fineberg [10] on PMMA/PMMA interface and Baumberger and Caroli [6] on gel/glass systems, suggest that the answer might lie in the evolution of stress profile along the interface prior to slip. Adding to this challenge is the issue of scaling laboratory based observations to earthquakes [25].

2.5 Research Statement

This study focuses on the microsecond time-scale events during onset of sliding friction in rough bimaterial interfaces. Traditionally, frictional sliding was treated as slow phenomenon at the interface. With the development of rate and state friction models, friction coefficient is not only dependent on normal stress but also of sliding velocity, and history of slip along the interface. Recent experimental studies demonstrate the dynamic nature of processes along the interface. Characteristic rupture waves have been observed in homogeneous and bimaterial interfaces at slow sliding as well as high impact speeds. Sources of perturbations are unknown and need further investigation. The prevailing question is if the nature of perturbation along the interface is shear crack-like or pulse-like? While crack-like model of rupture propagation is commonly accepted, dynamic impact experiments by Lykotrafitis et al. and numerical studies by Coker et al. as well seismic measurements [8, 21], show the existence of pulse-like propagation modes under certain conditions. Inversion of seismic data also support pulse-like model due to an order of magnitude difference in slip and heat generation. No clear demonstration of role of interface waves and their associated relative slip at slow sliding speeds exist.

In order to address the shortcomings, this research uses a combination of photoelasticity and Digital Image Correlation, to monitor wave propagations and their associated slip during stick-slip events along incoherent bimaterial interfaces. Mismatch in wave speeds along the interface resembles that of tectonic faults. The local stress fields along the interface is monitored to observe the detachment process and the associated rupture velocities. Using intermediate sliding speeds ranging

from 0.5 mm/s to 2.2 mm/s, bimaterial pair of PU on PMMA were investigated under constant uniform normal stress and tangential sliding velocity. Origin of rupture waves was also investigated. By introducing alternate frictionally weak zones along a bimaterial interface, the role of waves in triggering slip onset was investigated.

CHAPTER 3

EXPERIMENTAL METHODS

This chapter presents details on the experimental approach used to observe and measure frictional sliding parameters. Descriptions of in-house built friction test frame, sample preparation methods, and experimental procedures are provided. Full-field techniques of photoelasticity for stress analysis and Digitial Image Correlation (DIC) for in-plane strain field mapping were implemented. Simultaneous acquisition of both stress and strain mapping enabled visualization of the sliding event.

3.1 Sample Preparation

Polyurethane (PU) and poly(methyl methacrylate) (PMMA), also known as Plexiglas, were chosen as sliding pairs due to the mismatch in wave speeds. Clear transparent PU samples of Shore A 50 hardness were cast in the lab using the two component compound, Clear Flex 50 from Smooth-On Incorporation. Polished aluminum mold was used to cast PU samples of 76 mm by 38 mm and thickness of 10.20 mm. Vacuum degassing was performed on the mixed compound to obtain samples without

any trapped pores. Cast samples were cured for 20 hours at 70°C. After removing from the mold, the samples were milled to 75 mm by 37 mm by 10 mm. Plexiglas sample was milled to final dimensions of 125 mm by 60 mm by 12 mm. Both specimens were wet polished on abrasive sheets of grit sizes 120, 240, 360, and 600. Mitutoyo Surftest SJ-210 was used to measure surface roughness of PU and PMMA specimens. Average values of surface roughness (R_a) for PU and PMMA are 3.25 μm and 0.48 μm, respectively.

Theoretical values of longitudinal (c_l) and shear wave (c_s) speeds in a material can be obtained using the following relations, $c_l = \sqrt{\frac{E}{\rho}}$, and $c_s = \sqrt{\frac{\mu}{\rho}}$, where 'E' is the Young's modulus, 'μ' is shear modulus, and 'ρ' is the density. Acoustic methods can be used to experimentally determine the values of c_l and c_s in materials. One such technique is the Ultrasonic Pulse Echo Method, where the time-of-flight for piezo generated longitudinal and shear waves are measured in specimens of known thickness. Panametrics 5077PR pulser receiver module fitted with 10 MHz transducer was used to measure the wave speeds in PMMA. The values of measured wave speeds in PMMA were c_l = 2712 m/s and c_s = 1386 m/s. Wave speeds in PU could not be determined using this technique, due to high wave attenuation and dispersion. Theoretically estimated wave speeds in PU were c_l = 167 m/s and c_s = 98 m/s. Ratio of wave speeds in PU-PMMA bimaterial pair exceeds 15 times. PU was chosen in the study due to the slow speed of waves.

3.2 Photoelasticity

Photoelasticity is a full-field, non-destructive technique for visualization of stresses in materials which exhibit the property of birefringence. Such materials are called photoelastic materials. Many polymers such as PU, PMMA, and polycarbonate exhibit birefringence. Photoelastic materials undergo change in refractive index along principal stress axes when stressed. As polarized light passes through a stressed photoelastic specimen, the waves are preferentially slowed down along the normal to principal stress direction, leading to the formation of fringes. The relationship between fringes and stresses in the material can be obtained from equation (3.1), where f_σ is the fringe constant (determined from experiments on known stress states), N is the fringe number, and τ_{max} is the maximum shear stress in the specimen.

$$\sigma_1 - \sigma_2 = 2\tau_{max} = N f_\sigma \tag{3.1}$$

Fluctuations in shear stress along frictional sliding interface were visualized using photoelasticity. Figure 3.1 shows the schematic of dynamic photoelasticity setup. A 15 mW randomly polarized He-Ne continuous laser (λ = 633 nm) was used as a monochromatic light source. A Keplerian beam expander with spatial filtering and collimator was used to obtain a 50 mm collimated laser beam. The collimated beam was circularly polarized using an arrangement of quarter–wave plate and polarizer. The circularly polarized beam passed through an arrangement of specimen, analyzer, and quarter-wave plate. High-speed camera (IDT XVision XS-4) was used to capture the photoelastic fringes at 44,000 frames per second. The XS-4 has a 512 x 512 pixels CMOS sensor with 8-bit greyscale color depth and 2 GB

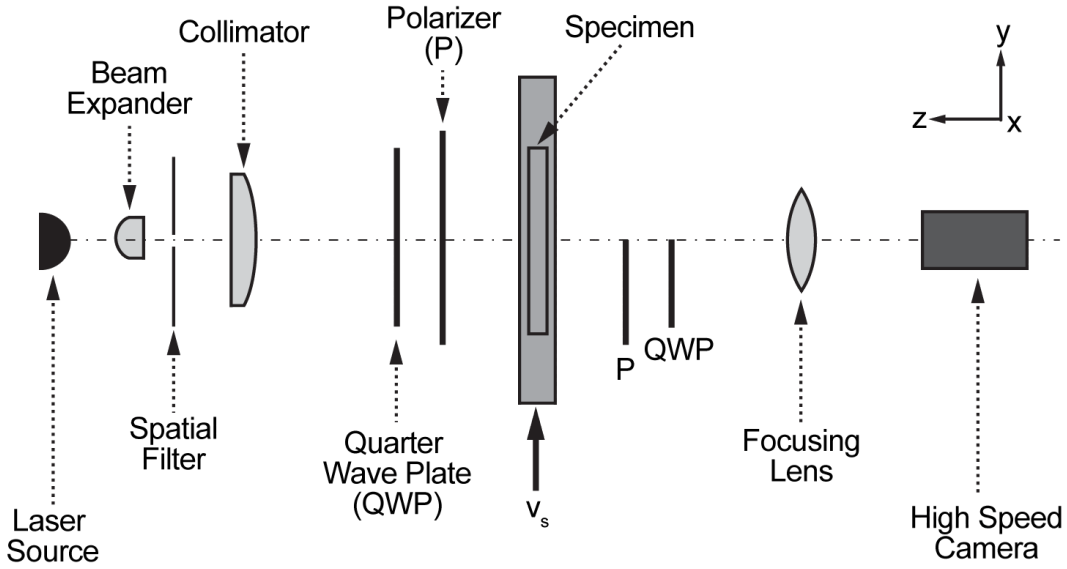

Figure 3.1: Schematic of dynamic photoelasticity used for real-time visualization of variation in shear stress along the interface during slip.

onboard storage. To reach framing rates of 44,000 frames/s, the image resolution was reduced to 56 x 512 pixels. The camera was triggered manually, along with 25% pre-trigger, upon the first occurrence of slip.

In order to obtain quantitative values of change in shear stress along the sliding interface, photoelastic analysis of fringes was conducted. Principle stresses in two-dimension can be expressed as:

$$\sigma_1, \sigma_2 = \left(\frac{\sigma_x + \sigma_y}{2}\right) \pm \sqrt{\left(\frac{\sigma_x + \sigma_y}{2}\right)^2 + \tau_{xy}^2}$$

In block and slider case, constant normal load is applied on the top block. We assume that the top slab has negligible lateral stress, i.e. $\sigma_x = 0$, while normal stress

is, $\sigma_y = F_N/A$.

$$\sigma_1, \sigma_2 = \frac{\sigma_y}{2} \pm \sqrt{\frac{\sigma_y^2}{4} + \tau_{xy}^2} \tag{3.2}$$

Substituting the values of σ_1 and σ_2 from (3.2) to (3.1), we get

$$\begin{aligned}
\left(\frac{\sigma_y}{2} + \sqrt{\frac{\sigma_y^2}{4} + \tau_{xy}^2}\right) - \left(\frac{\sigma_y}{2} - \sqrt{\frac{\sigma_y^2}{4} + \tau_{xy}^2}\right) &= N f_\sigma \\
2\sqrt{\frac{\sigma_y^2}{4} + \tau_{xy}^2} &= N f_\sigma \\
\sqrt{\frac{\sigma_y^2}{4} + \tau_{xy}^2} &= \frac{N f_\sigma}{2} \\
\frac{\sigma_y^2}{4} + \tau_{xy}^2 &= \left(\frac{N f_\sigma}{2}\right)^2 \\
\tau_{xy}^2 &= \left(\frac{N^2 f_\sigma^2}{4}\right) - \frac{\sigma_y^2}{4} \\
\tau_{xy} &= \sqrt{\left(\frac{N^2 f_\sigma^2}{4}\right) - \frac{\sigma_y^2}{4}}
\end{aligned}$$

Shear stress along the sliding interface estimated from fringe data is given by,

$$\tau_{xy} = \frac{1}{2}\sqrt{N^2 f_\sigma^2 - \sigma_y^2} \tag{3.3}$$

From existing literature, we know the value of f_σ for polyurethane to be 0.18 MPa.mm/fringe. Value of shear stress τ_{xy} can be determined for known values of fringe order number, fringe constant, and normal stress. Coefficient of friction (μ) can be determined by substituting the above derived relationship in Amontons

friction law.

$$\mu = \frac{\tau_{xy}}{\sigma_y} = \frac{\frac{1}{2}\sqrt{N^2 f_\sigma^2 - \sigma_y^2}}{\sigma_y} = \frac{1}{2}\sqrt{\frac{N^2 f_\sigma^2}{\sigma_y^2} - 1} \tag{3.4}$$

3.3 Digitial Image Correlation (DIC)

DIC is a non-contact, full-field technique, often exploited to track deformation of a surface, in experimental solid mechanics developed by Sutton et al. [38]. IDT XS-4 high speed camera was used to capture images of the target surface as it underwent deformation. The acquired images were compared with a reference image to compute displacements and their gradients. For the tracking algorithm to work efficiently, random surface features called as speckles were created either by spray painting or coating the surface. Size of speckles governed the resolution of this measurement technique. Figure 3.2 shows undeformed (P_0) and deformed (P_1) surfaces with speckle patterns. The basic assumption in DIC is that the greyscale value of speckles do not change after deformation, although recent DIC codes accommodate small changes in greyscale values. Instead of comparing individual pixel values, a small subset of the image was chosen and the pattern was searched in the deformed image. Discrete greyscale values of pixels comprising the subset image were curve-fitted (quadratic or cubic smoothing) to obtain continuous surface profiles. This technique, called as sub–pixelation, enabled tracking of deformations in the order of fraction of a pixel. Gradual variations in greyscale intensities are preferred in order to obtain a smooth and continuous surface fit. This can be achieved by slightly defocussing the camera lens during acquisition or by spray painting black paint over a thin coating of wet white paint. In-house developed 2D-DIC program was used in this study. More

details on this code be found in following journal article by Lu and Cary [22].

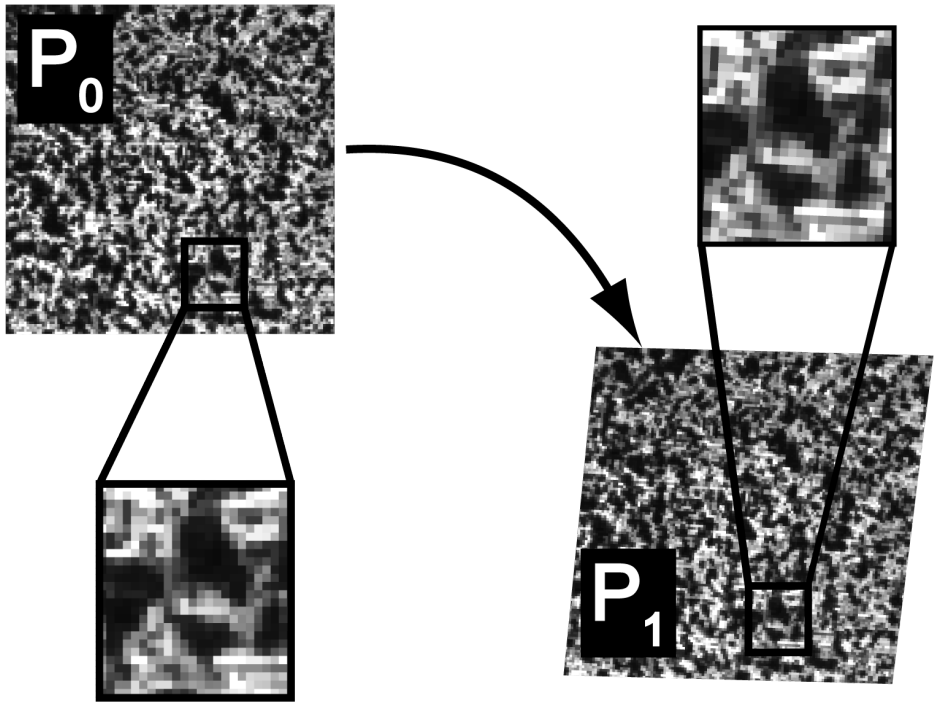

Figure 3.2: Schematic of Digital Image Correlation (DIC) used for tracking in-plane deformation of a surface coated with random speckle pattern. P_0 is the undeformed state, while P_1 is the deformed state. Correlation subset is indicated in the magnified box.

3.4 Two-axis Friction Test Apparatus

Frictional sliding tests were performed using an in-house designed and built test frame shown in Figure 3.3. Figure 3.4 shows the schematic of the test fixture. The fixture was designed to implement the block and slider friction model. Dead weights (ranging from 25.7 to 50.7 lbs) were used to apply constant normal force on the test specimens. The top block was held to the load plate using cyanoacrylate glue preventing any sliding during experimentation. Top loading plate was free to slide in

the vertical direction on four precision stainless shafts (diameter = 1 inch) while its motion was constrained in the horizontal axis.

Slow sliding of the lower block was induced by a 0.5 HP Baldor DC brushless servo motor (DBSM33C-177MHQ) driving a linear actuator (Joyce Dayton IA201-TT-6-LJ10-MMAX-X) with linear travel of 150 mm. Velocity of the linear actuator was varied using a motor controller allowing constant sliding velocities ranging from 0.4 mm/s to 2.8 mm/s. The bottom specimen was adhesively constrained to a platform resting on precision bearings and shafts with estimated friction coefficient of 0.001. For low modulus materials such as polyurethane, constant normal loading using dead weights was used. For higher modulus materials such as polycarbonate and plexiglas, which also have lower fringe sensitivity, it is difficult to generate high normal loads using dead weights. An Acme threaded shaft was used to generate desired normal load and then locked in position using lock nuts. Static 1000 lbs load cells with 5.2 KHz resonant frequency were used to measure the normal and shear loads. However, no shear force measurements were performed due to lack of sensitive dynamic load cells at the experimental facility for soft materials like PU.

Speckle patterns were created on one-half region of PU sample, using quick-drying black spray paint. These speckles were used for tracking particle displacements using Digital Image Correlation (DIC). PU-PMMA material pair was loaded normally using dead weights and tangential loading was applied on the bottom PMMA clock , using linear actuator. The whole sequence of events were captured using a high speed camera at 44,000 frames per second. Each image,

8-bit greyscale TIFF, was 81 pixels in height and 512 pixels in width. The image files comprised of isochromatic fringes as well as deformation of speckle patterns in polyurethane sample close to the interface. Due to lower fringe sensitivity of plexiglas, no fringes were recorded. The high speed camera was triggered manually using pre-trigger delay, thereby facilitating the capture of the first slip event. A sequence of 75,000 images were acquired for each test representing a total duration of $\sim$1.7 seconds. A total of 900 images before and after the slip onset were chosen for particle displacement and velocity analysis using DIC.

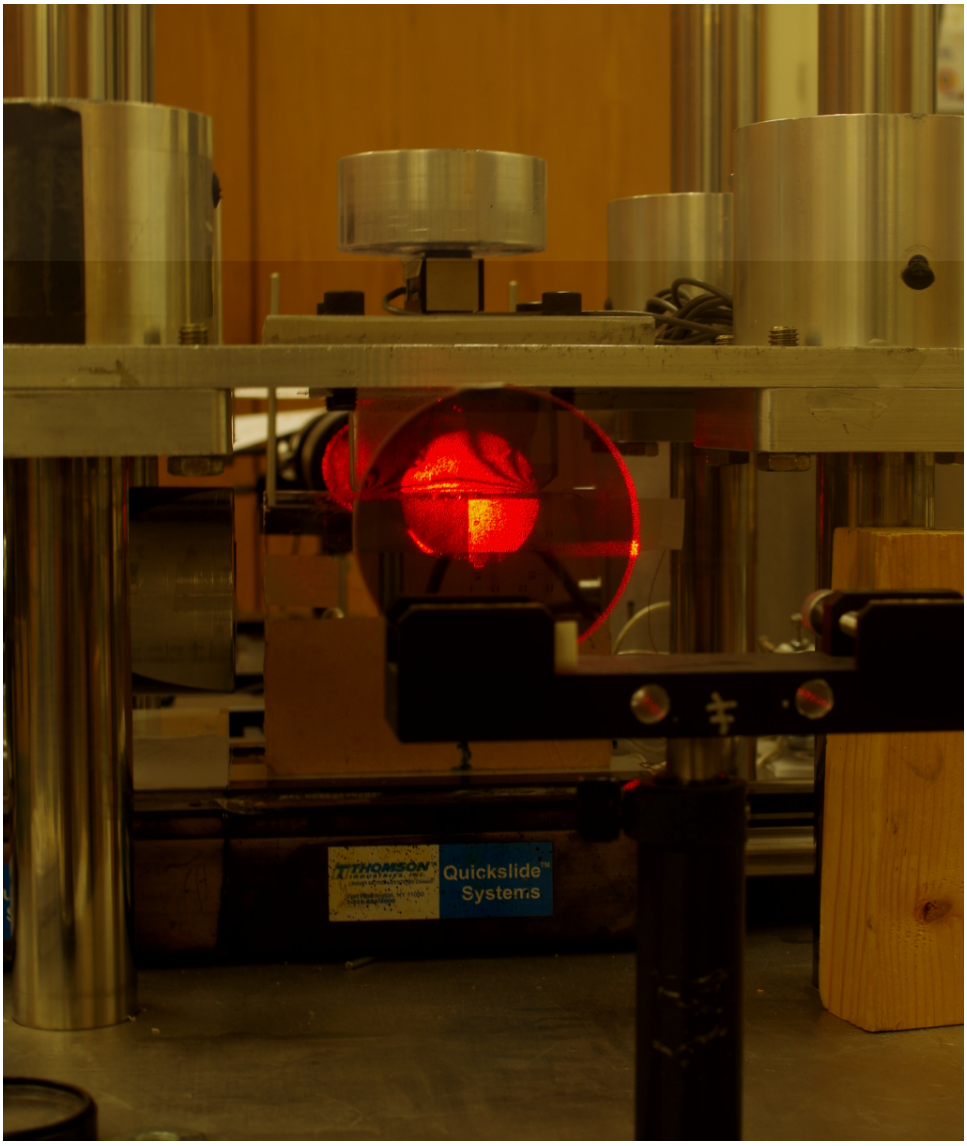

Figure 3.3: Front view of the two-axis friction test setup in operation. Top loading plate is supported by frictionless bearings allowing only vertical motions on the precision stainless steel shaft. Tangential slider driven by a servo motor to impose the shear loading of the PMMA sample. Circular polarizer shows photoelastic fringes in PU-PMMA sliding pair, illuminated by 50 mm He-Ne laser beam.

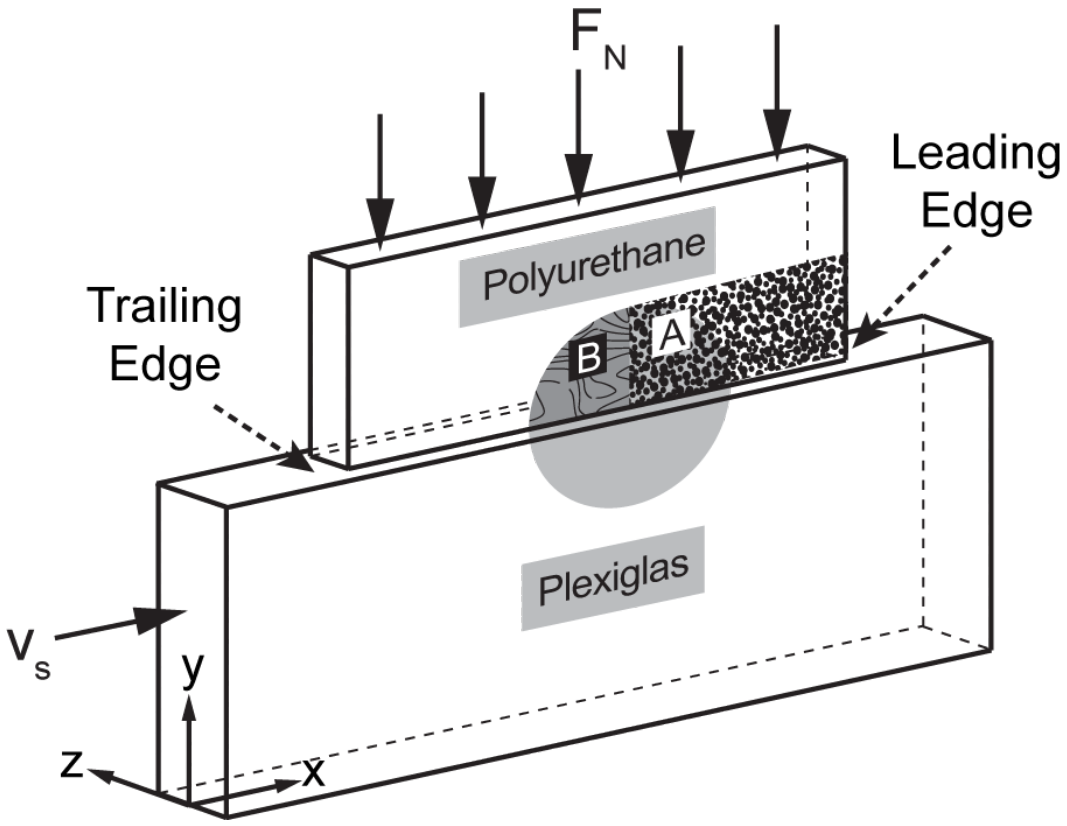

Figure 3.4: Schematic of frictional sliding setup with constant normal load (F_N) and sliding velocity (v_s). Region A– random speckle patterns on polyurethane specimen for Digital Image Correlation. Region B– isochromatic fringes on polyurethane specimen.

CHAPTER 4

RESULTS

In this chapter, the results of experiments conducted to investigate the role of stress perturbations with respect to onset of sliding are presented. High-speed image acquisition of dynamic photoelasticity combined with DIC were investigated in the frictional sliding pairs of PU on PMMA for three different sliding velocities and normal loads. The test variables, namely, sliding velocity and normal load, are shown Table 4.1. Each test case was a unique combination of the two experimental variables. The sliding pair of PU on PMMA is kept constant. Dynamic photoelasticity and DIC analysis were performed on the high-speed camera images for each test case. Images from high-speed camera showed successive stick slip events, from which the stick-slip frequencies were calculated, as seen in figure 4.1. Stick-slip frequency increased with sliding velocity and decreased with increase in normal load. Since, stiffness of the loading frame affects stick-slip, it is worthwhile to note that the load frame can be assumed as rigid. Within each stick-slip event, the evolution of slip phase was investigated.

Figure 4.1 shows the stick-slip frequency for the sliding of PU–PMMA as a

function of normal load and slider velocity. Stick slip are dynamic oscillatory events in frictional sliding caused by a variety of factors that ranges from the bulk properties of the sliding pairs to stiffness of the imposed tangential sliding. Our experiments shows that at low slider speeds and low loads, the material pair of PU–PMMA exhibit low stick-slip frequencies. As sliding velocity increased, the stick-slip frequency increased but not infinitely. After reaching certain velocities and beyond, sliding becomes continuous and stable. In this study, our focus is to investigate the events prior and during stick-to-slip-to-stick transition. Hence, determination of stable slider velocities has not been pursued. In order to understand the dynamical behavior of the sliding system in hand, the values of stick-slip frequencies have been reported here. Based on trends reported in Figure 4.1, we find that the slider velocity has a more pronounced effect on stick-slip frequency at higher normal loads. This shows that normal load has a more pronounced effect on stick-slip sliding as opposed to slider velocity. In seismic studies, every slip event is considered as an earthquake occurrence. Although, it is possible to monitor and measure the rate of sliding of tectonic plates, the ultimate key to predicting the occurrence of earthquakes lie in our ability to determine the point in time when stick-to-slip transition occurs. In this pursuit, we investigated sliding pairs in controlled laboratory scale to understand the shear stress evolution over time at different sliding velocities and normal loads.

4.1 Observation of Rupture Cascades Prior to Slip Onset

A sequence of multiple stick-slip events were recorded within the acquisition duration of 1.6 seconds. A stick–slip–stick sequence was isolated and analyzed. Figure 4.2

Table 4.1: Test cases for unique combinations of the two test variables, namely, sliding velocity and normal load.

Test Case	Sliding Velocity (mm/s)	Normal Load (N)	Normal Stress (MPa)
V1-P1	0.5	114	0.15
V1-P2	0.5	159	0.22
V1-P3	0.5	226	0.30
V2-P1	1.5	114	0.15
V2-P2	1.5	159	0.22
V2-P3	1.5	226	0.30
V3-P1	2.2	114	0.15
V3-P2	2.2	159	0.22
V3-P3	2.2	226	0.30

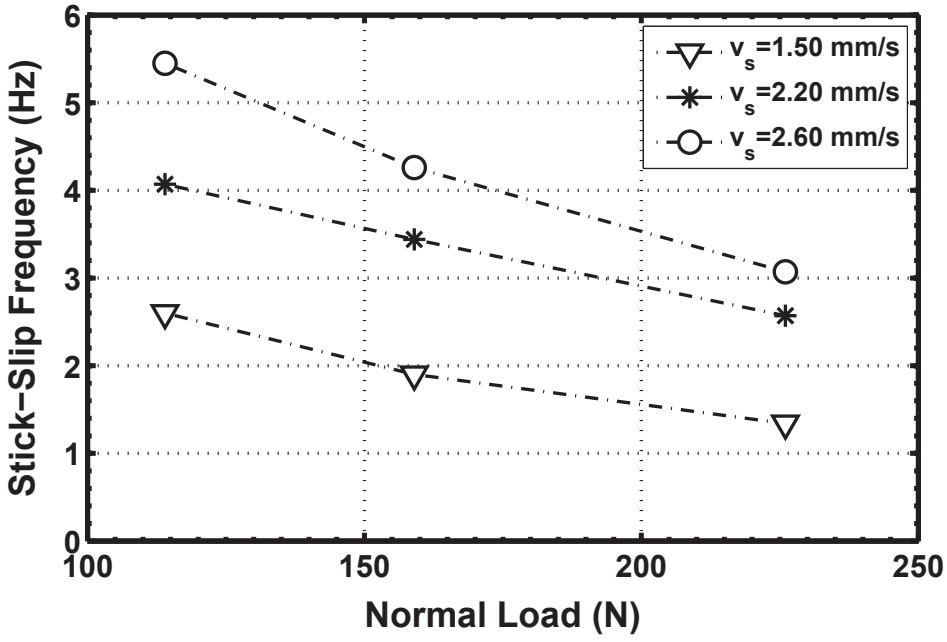

Figure 4.1: Stick-slip frequency as a function of normal load and sliding velocity, obtained from analysis of slip events from high-speed camera images.

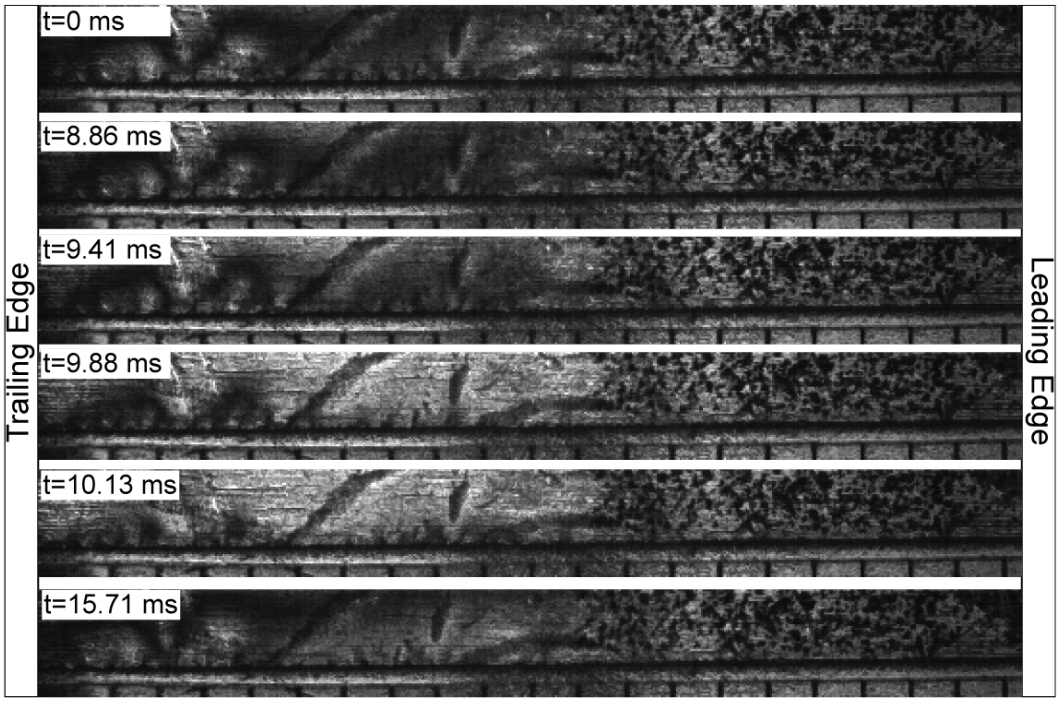

Figure 4.2: Sequence of images from test case V1-P1 (v_s= 0.5 mm/s and F_N= 114 N). Isochromatic fringes show variation in shear stresses along the interface at different times.

shows the raw images obtained from the test case V1-P1 (v_s= 0.50 mm/s and F_N= 114 N). Visual inspection of photoelastic fringes along the interface, revealed the following order of events. At time t= 0 ms, multiple fringes representing shear stress build-up along the interface were observed. These fringes remained constant until t= 8.86 ms, when a small drop in shear stress was observed. This is associated with the passage of p-wave from leading to trailing edge. At 9.41 ms, drastic drop in shear stress along the interface begins, representing the passage of s-wave. Sliding of the PU specimen was observed between 9.41 and 15.71 ms. This marked the beginning of the slip phase. A single slow front followed by multiple wave fronts originating from the leading edge were observed prior to large scale sliding. Upon

passage of the slow fronts, the fringes along the interface completely vanished, denoting interface detachment or drop in shear stress. At 15.71 ms, pinning of the interface began and the fringes re-emerged. During the stick phase, increase in shear stresses occurred as the lower PMMA specimen continued to slide at v_s= 0.5 mm/s. The rate of increase in shear stress was orders of magnitude as compared to the drop in shear stress while slip onset. Fineberg et al. [32, 34] observed propagation of similar wave fronts in their quasistatic sliding experiments on PMMA-PMMA pair. Although, they reported the propagation of p-wave, s-wave, and then slow sub-Rayleigh front, we find that multiple fronts propagated along the interface during the slip process. The technique of contact area measurements using light transmission along the interface, as adapted by Fineberg et al., is sensitive to points along the interface that separate physically. Such physical detachment of the interface is usually caused by opening pulses/cracks. In our study here, we observe ruptures as function of shear stress along the interface. A physical separation or opening is not necessary for a shear crack/pulse to propagate. But both experiments confirm the dynamic nature of events leading to sliding between two interfaces even if the loading conditions are quasistatic.

In order to derive quantitative information on the location and velocity of various rupture fronts, a special image was constructed from a row of pixels close to the interface from all 900 images. By stacking the individual row of pixels, a spatio-temporal image was created. Such spatio-temporal plots were used by Baumberger et al. to study slip sequences in gel-glass interface [6]. Figure 4.3 shows one such plot for the test case of V1-P1. Horizontal axis represents the spatial location of the

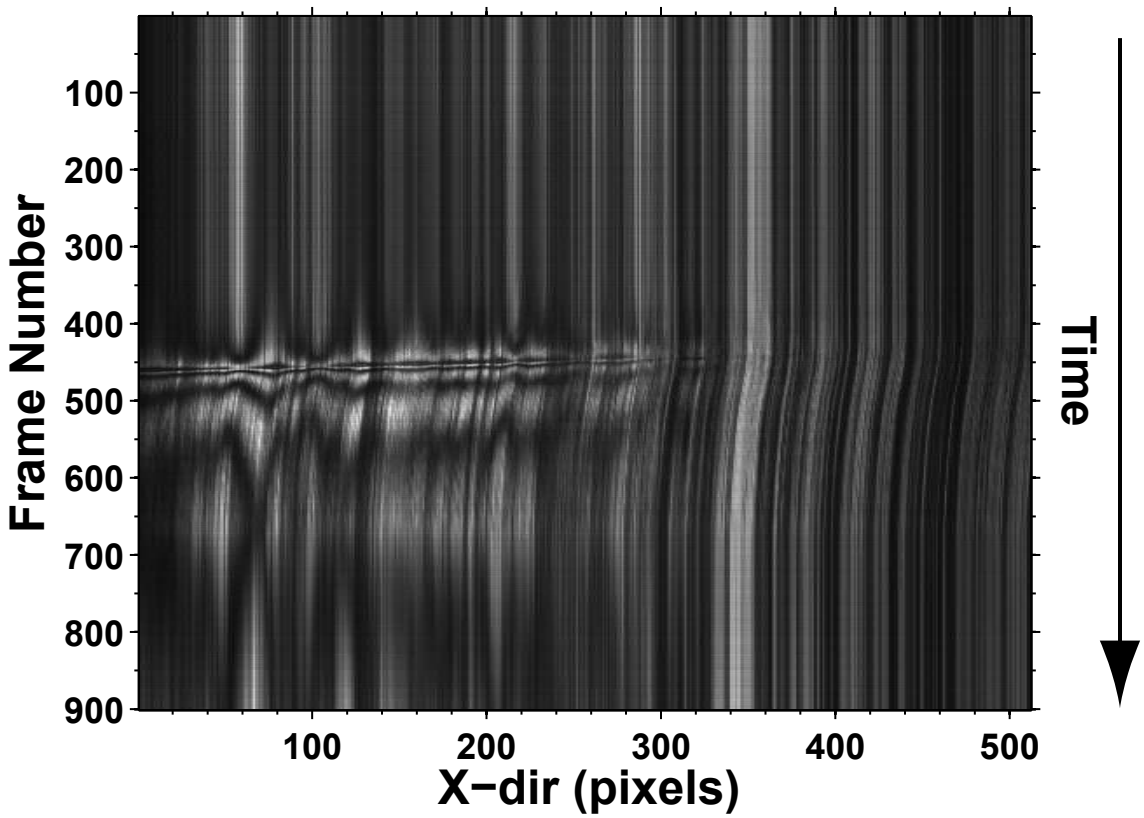

Figure 4.3: Image constructed by extracting a row of pixels, close to the interface, and stacking them in sequence. 512 pixels in the horizontal axis represents 21 mm in length. Interframe time is Δt= 2.27 μs.

fringes in pixels units. Vertical axis represents the frame numbers of the extracted row of pixels. As the interframe time between images is known, Δt= 2.27 μs, time lapse between frames can be calculated. Velocity of the rupture fronts were be determined from this plot. From the plot, we observe no change in pixel intensity until around 400$^{\cdot}$th frame. Rupture fronts along the interface propagated from leading to trailing edge between frames #415 to #550. A clear rupture front was observed at frame #450. This represented the slow front propagating along the interface. Velocity of slow shear-like wave front was found to be in the order of

40 m/s, which is about $0.3c_s$ to $0.4c_s$ for PU. We also observed slip onset from the changes in greyscale values of speckles. Speckle patterns lay between 375 and 512 pixels. DIC analyses of the speckle patterns provided detailed information on the onset of sliding, including the magnitude of slip and instantaneous velocity.

Although, characteristic wave fronts were identified, the question of origin of the rupture fronts prevails. By assuming that a single point source emanating s-wave and sub-shear wavefronts, it is possible to estimate the approximate location of the origin. Using the known wave velocities for s-wave and sub-shear fronts, the origin can be traced. In the observation window, the two wave fronts were separated by 9 frames. Origin of rupture was traced to a point close to the leading edge. Actual experimental observations have been performed in this study to confirm the source of rupture fronts as well. The results are discussed later in this chapter.

Figure 4.4: Nodal locations comprising a linear grid for DIC analysis. The nodal points are separated by 10 pixels in the horizontal direction.

4.2 DIC Analysis of Stick to Slip Transition

DIC analysis was performed at discrete nodal locations close to the interface (about 1 mm above the sliding interface). The nodes lay in straight line parallel to the interface, separated by 10 pixels (0.4 mm apart), as seen in figure 4.4.

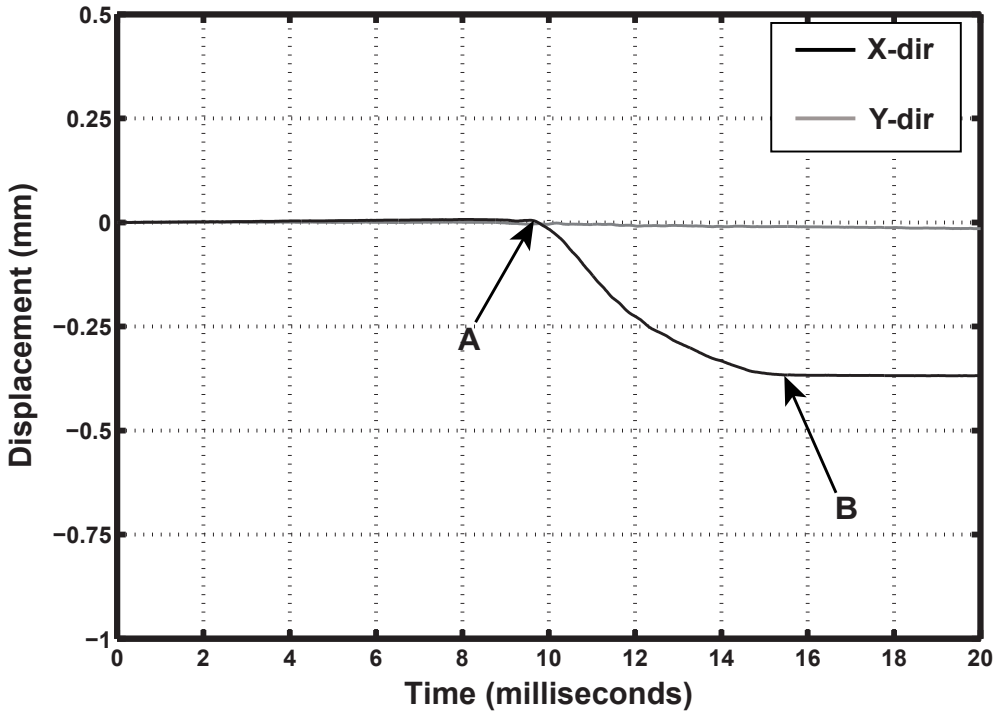

Figure 4.5: Displacement history of a node obtained from DIC analysis of stick-slip event in test case V1-P1. The dark line represents displacement along X-dir. The lighter greyline represents displacement along Y-dir. Onset of slip is denoted by point A, and end of slip is denoted by point B. Duration of slip phase is $\sim$6.3 ms and slip magnitude is 0.39 mm.

Image correlation was performed at these nodal locations for all the 900 images. Upon successful correlation, the values of nodal displacements were obtained. Instantaneous values of displacement along X- (shear) and Y- (normal) directions as well as instantaneous velocities were calculated from the nodal locations. Figure 4.5 shows the displacement of a node along X- and Y- directions for test case of V1-P1. Onset of slip is denoted by Point A which corresponds to time,t= 9.8 ms. No detectable displacements were observed along Y-dir within the resolution of DIC algorithm. In the case of X-displacement (or tangential slip), it follows a non-linear

path. Duration of the slip was around 6.3 ms. After a rapid drop in X-displacement, it gradually come to rest. The magnitude of slip was 0.39 mm. During the slip phase, bottom interface (PMMA) displaced by 3.15 μm in the direction opposite to that of the slip in PU.

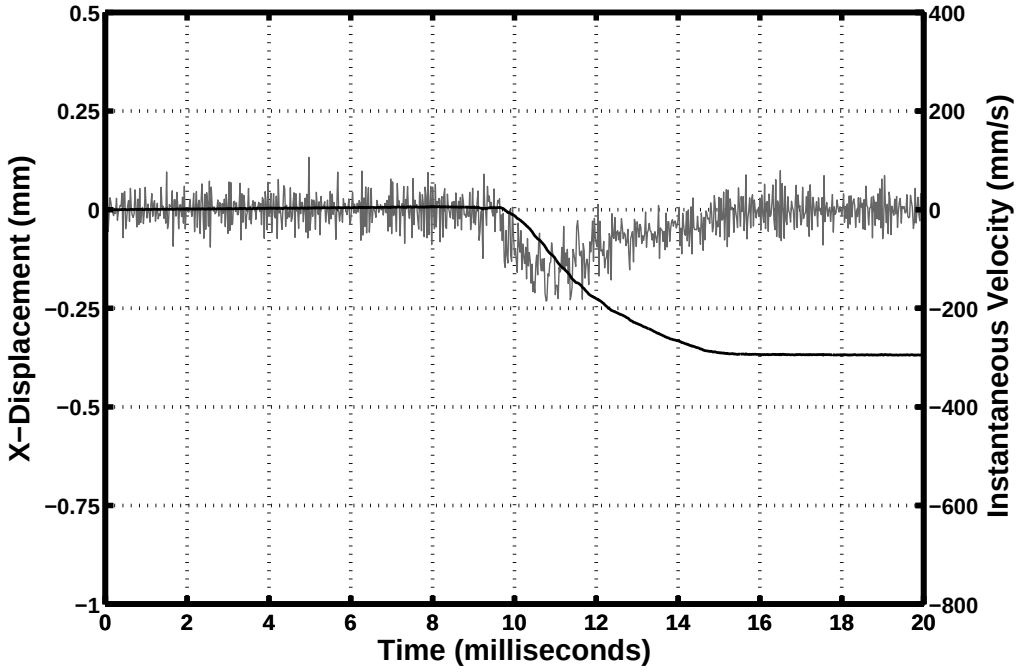

Figure 4.6: Plot of displacement and instantaneous velocity along X-dir at a node, obtained from DIC analysis of stick-slip event in test case V1-P1. The dark line represents displacement along X-dir. The lighter greyline represents instantaneous velocity along X-dir.

Instantaneous velocity was obtained by calculating the slope between two consecutive displacement values at each DIC node. Figure 4.6 shows the displacement and velocity profile, along X-direction, at a node during entire stick-slip-stick event. Oscillations in velocity during stick phase are due to the

discrete nature of displacement computation from DIC images. Spectral analysis of velocity in the stick phase, yielded no dominant frequency, indicating white noise. Smoothing/filtering technique of 9-point moving average was implemented to reduce spurious oscillations. Figure 4.7 shows the smoothed displacement and resulting instantaneous velocity profile. Further confirmation of slip onset at 9.80 ms was confirmed by the velocity profile. After a rapid rise in velocity to 170 mm/s (acceleration phase), the slip slows down to zero (deceleration phase). The durations of acceleration and deceleration phases are 1.8 ms and 4.1 ms, respectively. However, the magnitudes of slip in both phases are almost equal. The acceleration phase was governed by velocity weakening friction, where small increase in sliding velocity due to slip caused rapid drop in localized friction coefficient. After reaching high slip velocities of 200 mm/s, the sliding regime shifted to velocity strengthening mode, where the local friction coefficient strengthens over time. It is speculated that a combination of decrease in inertia and establishment of asperity contacts (pinning) leads to the onset of long and slow deceleration phase. Shear stress along the interface increase gradually until slip is arrested and the next stick phase begins.

Figure 4.7 shows the displacement profiles of all nodes for the test case of P1-V1. This figure shows the uniformity in slip in PU specimen. Delay in onset of slip is observed from the displacement profiles. From dynamic photoelastic fringes, the onset of sliding was initiated after the passage of slow sub-shear wave front. Average value of total slip for all the nodes was found to be 0.38 mm. Figure 4.8 shows the instantaneous velocity along X-direction for the test case of P1-V1. The duration of acceleration and deceleration phases are equal at all nodes. Average value of peak

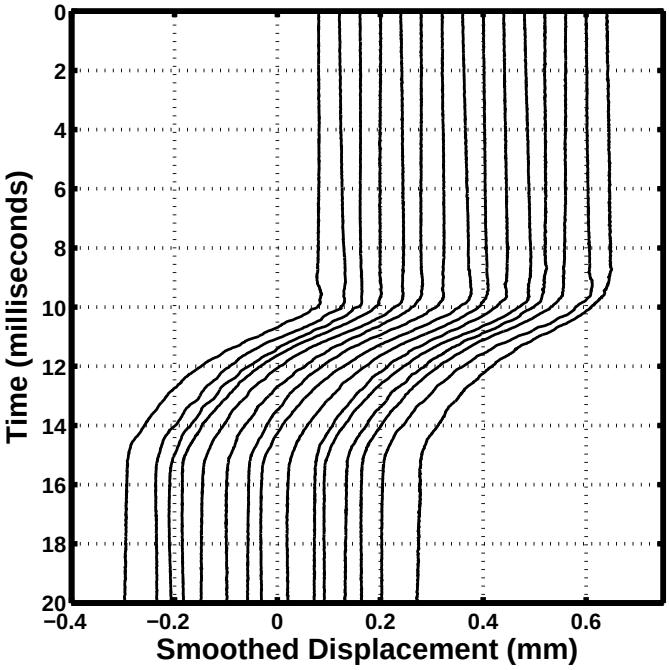

Figure 4.7: Plot of displacement profiles along (slip) X-dir at all nodes, obtained from DIC analysis of stick-slip event in test case V1-P1.

slip velocity of all the nodes was 149 mm/s.

Based on the experimental results reported above, we observe direct evidence of different rupture wave velocities and their associated slip magnitudes and durations in quasistatic loading conditions. Using the combination of DIC and photoelasticity, the entire stick-slip event has been characterized and quantified. We believe that such a detailed description of stick-slip event has not been reported yet.

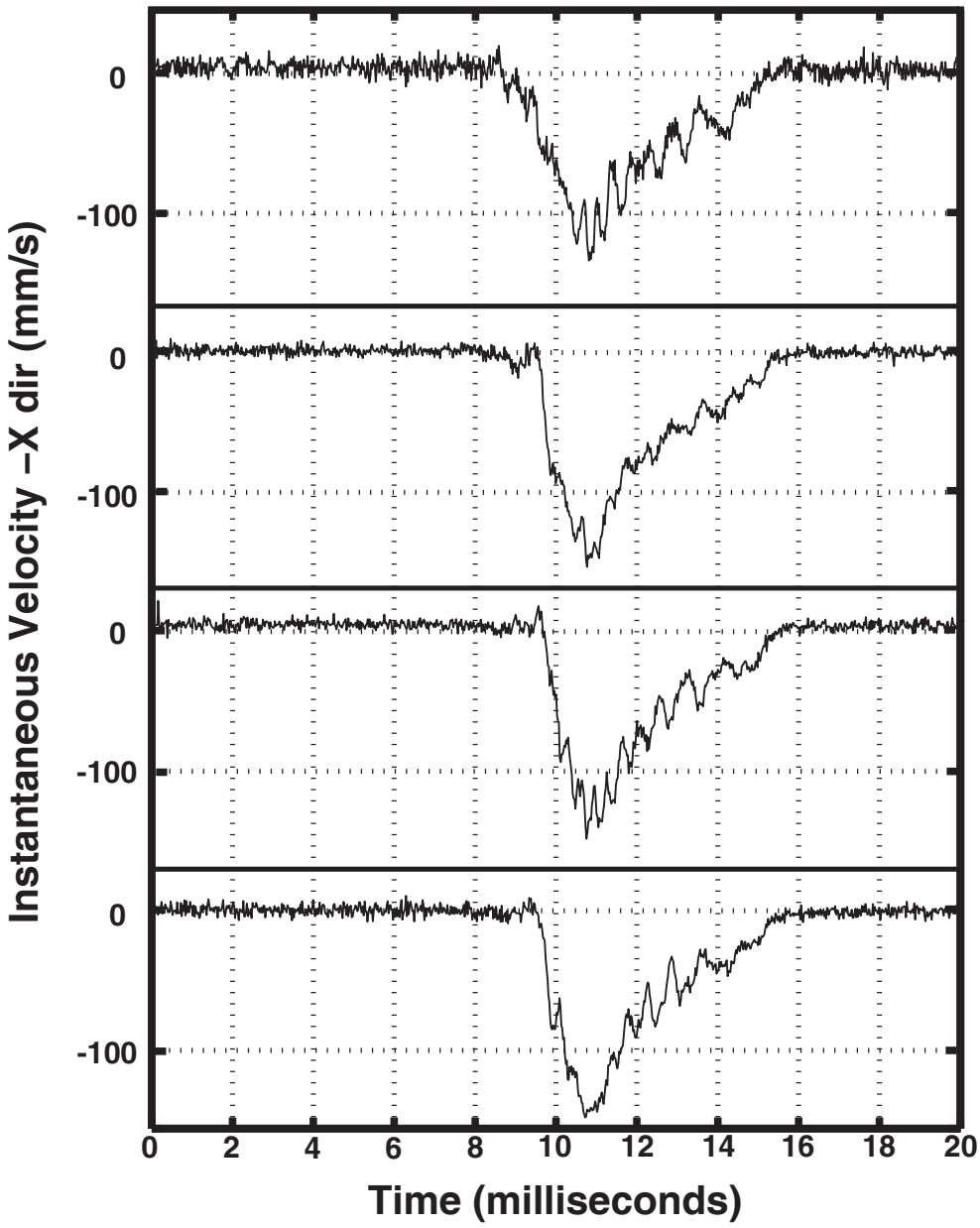

Figure 4.8: Plot of instantaneous velocities along X-dir at four nodes, obtained from DIC analysis of stick-slip in test case V1-P1.

4.3 Effect of Driving Velocity

In the previous section, we observed the onset of frictional sliding upon the propagation of three distinct wave fronts. In order to understand the effects of driving/sliding velocity, the normal load constant, while three different driving velocities were imposed, namely, 0.50, 1.50, 2.20 mm/s. The normal stress was maintained constant at 0.15 MPa by using dead weights (25.7 pounds).

Figures 4.9, 4.12,and 4.15 show the progression of interface waves for the three different driving velocities. We observe narrowing of the stress perturbation zone. At lowest velocity of 0.50 mm/s, the rupture interface is spans from frames #425 to #500. At driving speeds of 2.20 mm/s, the rupture interface was very narrow, from frames #350 to 400. Table 4.2 shows the comparative values of various quantities measured from high-speed image sequences and DIC. With increase in driving velocity, we see a drop in slip magnitude from 0.38 mm to 0.36 mm. Duration of slip dropped from 5.86 ms to 5.07 ms, with increase in velocity. Maximum velocity of slip remained unaffected, between 149 mm/s and 174 mm/s. This invariance of maximum slip velocity shows that this parameter is material dependent, such as elastic modulus or density inertial dependent. However, the velocity of wave across the interface is found to increase from 34 m/s to 82 m/s, with increase in driving velocity. Velocity of the slow wave front varied from $0.35c_s$ to $0.83c_s$ as driving velocity was increased. However, no intersonic fronts (wave fronts with velocity greater than shear wave speed) were observed in this study. Such intersonic fronts have been reported recently

Table 4.2: Comparison of measured quantities for three different sliding velocities and constant normal stress of 0.15 MPa.

Test Case	Sliding Vel. (mm/s)	Slip (mm)	Slip Duration (ms)	Max. Slip Vel. (mm/s)	Wave Vel. (m/s)
V1-P1	0.50	0.38	5.86	149	34
V2-P1	1.50	0.36	5.44	177	70
V3-P1	2.20	0.36	5.07	174	82

in the dynamic impact driven sliding experiments(Rosakis et al. 1999, Xia et al. 2004). Unlike the observations of Rubinstein (Rubinstein et al. 2006), we observe no intersonic fronts in this study. For slow driving speeds, no such velocity dependence has been reported yet.

4.4 Effect of Normal Stress

In order to investigate the role of normal stress on the frictional sliding behavior, we vary normal stress while keeping driving velocity constant. Three different normal stresses (σ_n) of 0.15 MPa, 0.22 MPa, and 0.30 MPa were chosen due to the low modulus of PU. Due to high Poisson's ratio of PU (close to 0.5) and low elastic modulus, swelling of the sample was observed at loads above 0.30 MPa. In case of earthquakes, normal stresses vary from 10 MPa to 100 MPa in the rocks near fault zones. Although, aim of these experiments are not to replicate earthquakes in lab-scale, we believe that the results can provide us valuable insights to various mechanisms in frictional sliding.

Figures 4.9, 4.10, and 4.11 show the propagation of slip pulses along the interfaces for test cases where the sliding velocity was kept constant at 0.50 mm/s. The onset of slip was dominated by the passage by the three distinct wave fronts, namely, p-wave, s-wave, and subsonic shear fronts. As normal stress increased, the magnitude of slip also increased. Perturbations along the interface increased as normal load was doubled. Table 4.3 shows the various parameters measured from the images and DIC analysis. Variation in normal stress had a profound effect on the slip magnitude. When the normal stress was doubled, the slip distance also nearly doubled; while the duration of slip increased by 1.25 times. The maximum velocity of slip was found to increase with normal stress, whereas the wave velocity was found to be nearly constant.

Table 4.3: Comparison of measured quantities for three different normal stresses and constant sliding velocity of 0.50 mm/s.

Test Case	Normal Stress (MPa)	Slip (mm)	Slip Duration (ms)	Max. Slip Vel. (mm/s)	Wave Vel. (m/s)
V1-P1	0.15	0.38	5.86	149	34
V1-P2	0.22	0.52	6.39	203	39
V1-P3	0.30	0.71	7.34	264	46

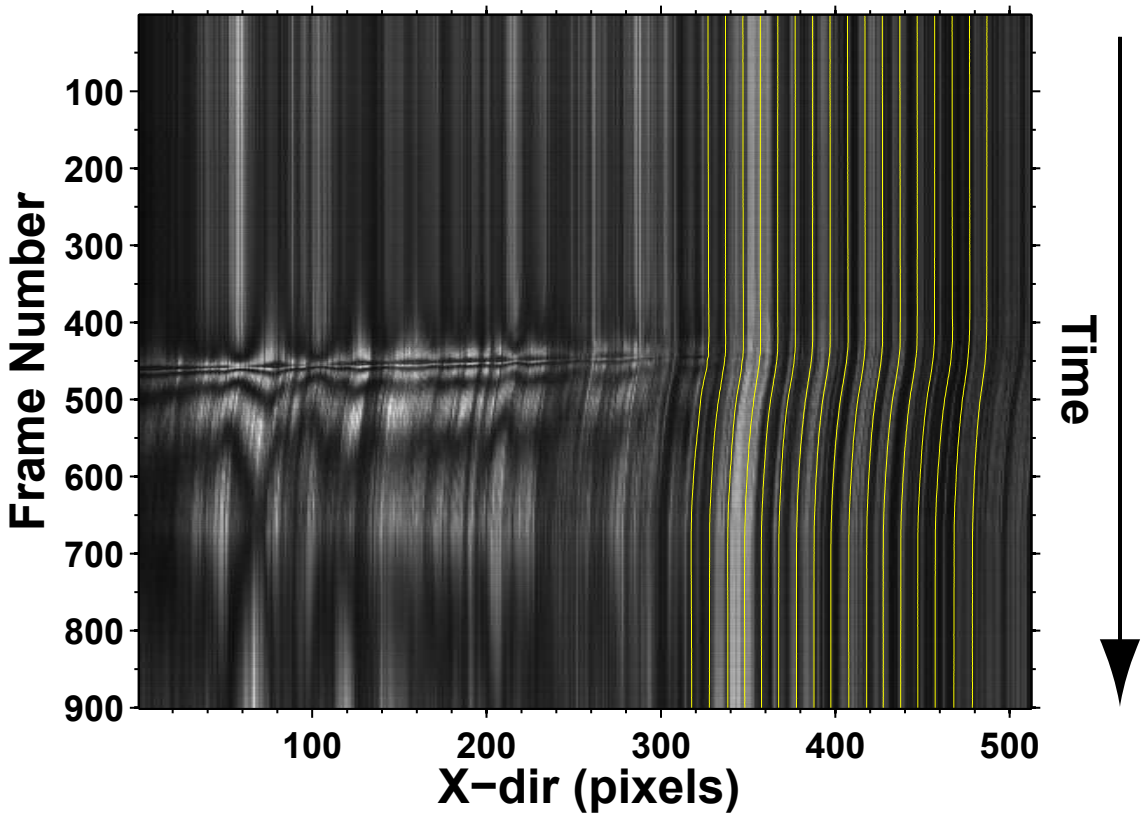

Figure 4.9: Image sequence for test case V1-P1, sliding velocity v_s= 0.50 mm/s and normal stress 0.15 MPa. Yellow traces are DIC tracked slip displacements.

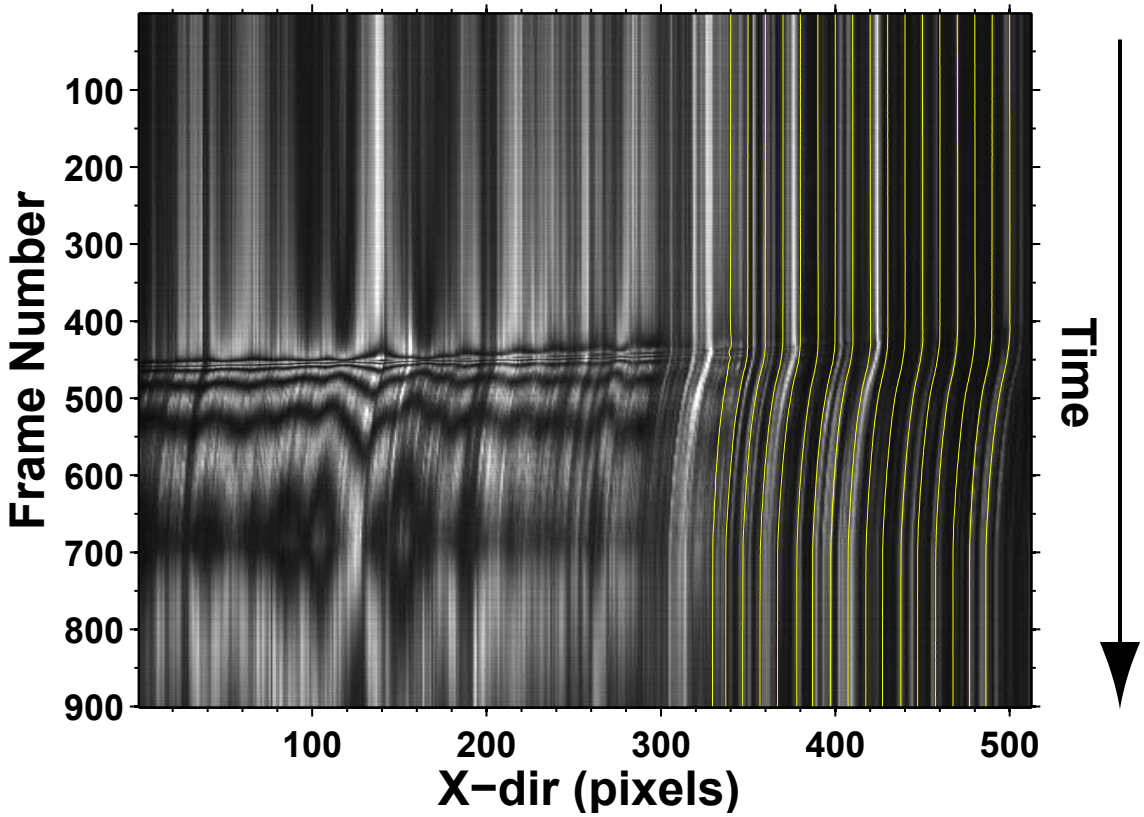

Figure 4.10: Image sequence for test case V1-P2, sliding velocity v_s= 0.50 mm/s and normal stress 0.22 MPa. Yellow traces are DIC tracked slip displacements.

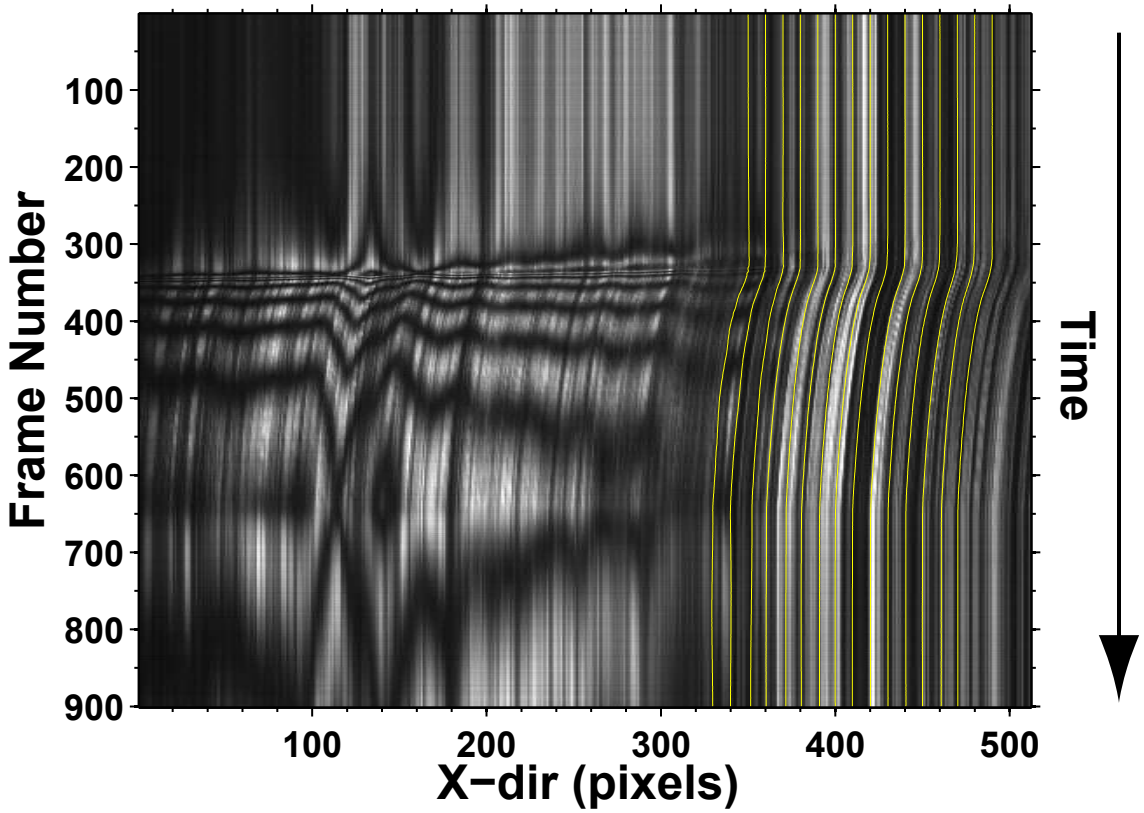

Figure 4.11: Image sequence for test case V1-P3, sliding velocity v_s= 0.50 mm/s and normal stress 0.30 MPa. Yellow traces are DIC tracked slip displacements.

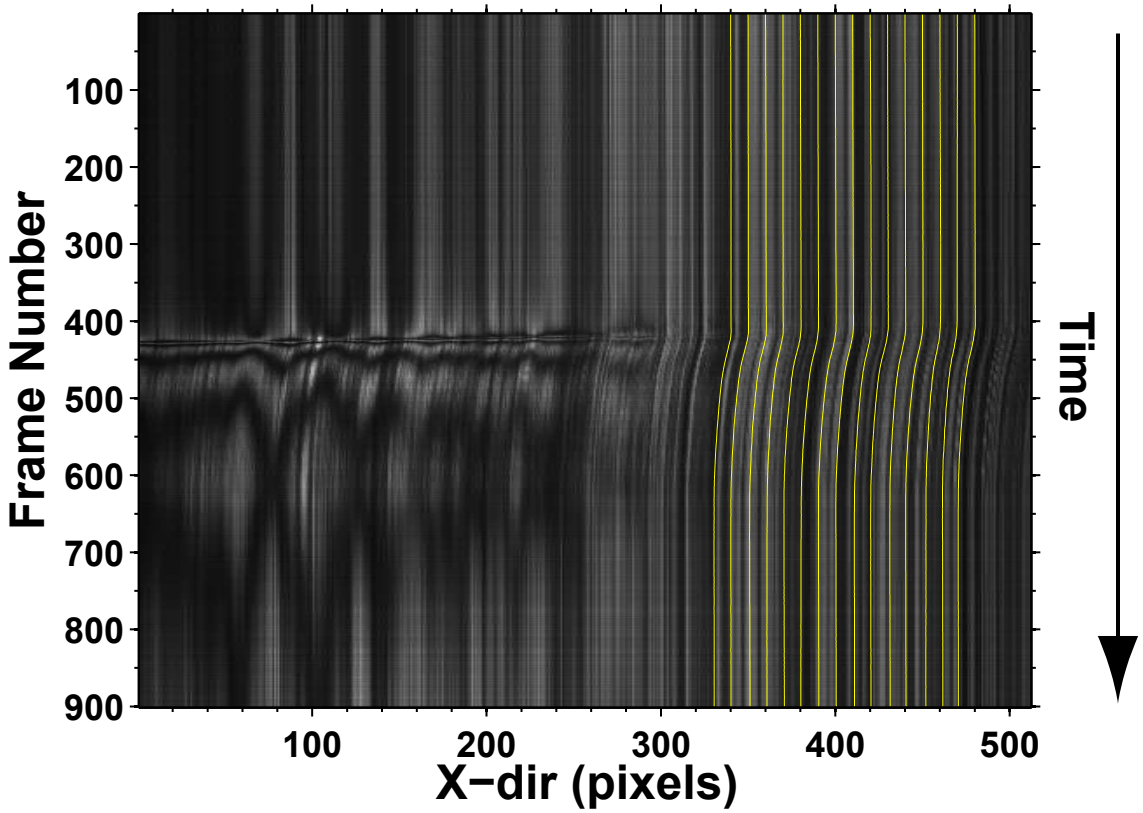

Figure 4.12: Image sequence for test case V2-P1, sliding velocity v_s= 1.5 mm/s and normal stress 0.15 MPa. Yellow traces are DIC tracked slip displacements.

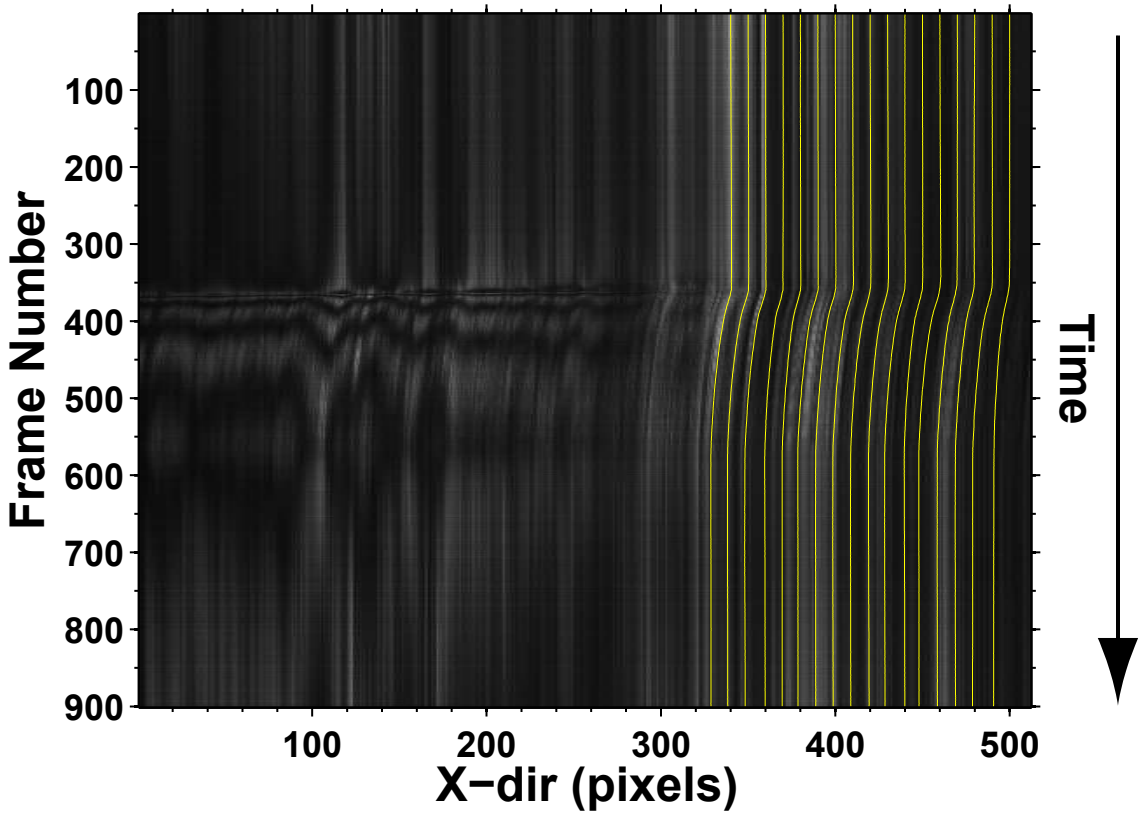

Figure 4.13: Image sequence for test case V2-P2, sliding velocity v_s= 1.5 mm/s and normal stress 0.22 MPa. Yellow traces are DIC tracked slip displacements.

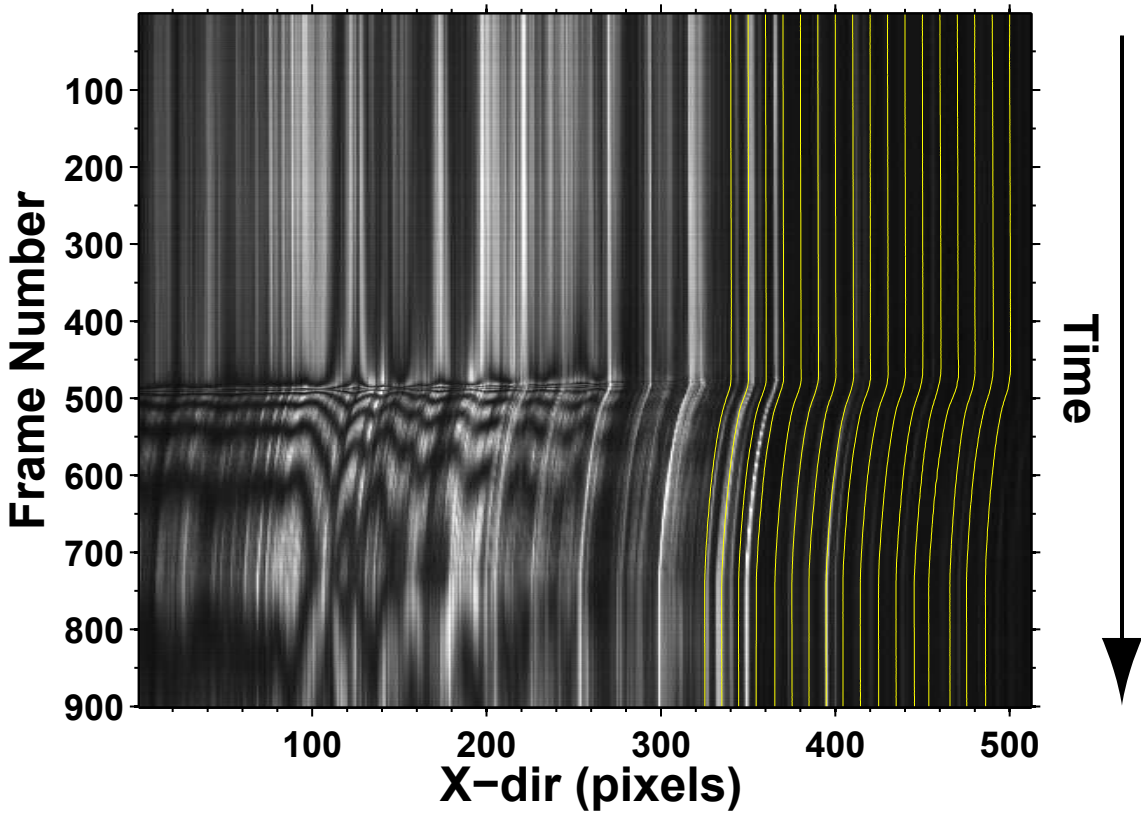

Figure 4.14: Image sequence for test case V2-P3, sliding velocity v_s= 1.5 mm/s and normal stress 0.30 MPa. Yellow traces are DIC tracked slip displacements.

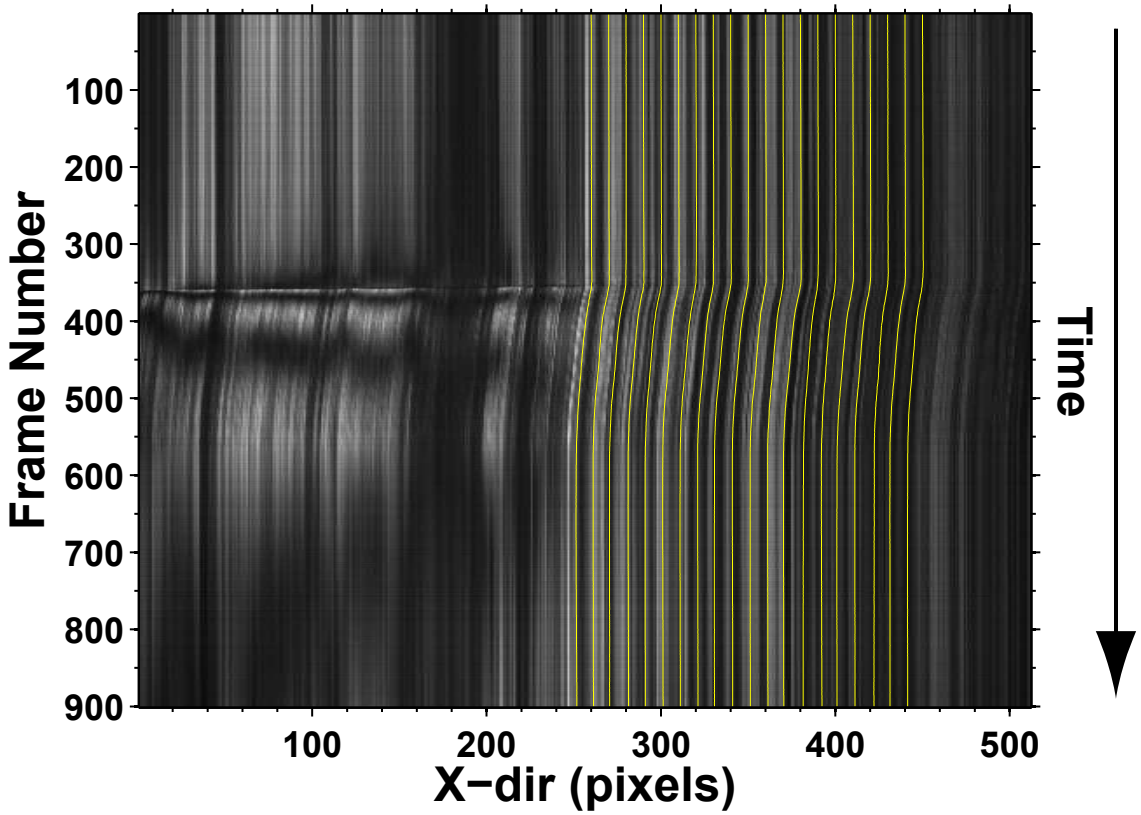

Figure 4.15: Image sequence for test case V3-P1, sliding velocity v_s= 2.2 mm/s and normal stress 0.15 MPa. Yellow traces are DIC tracked slip displacements.

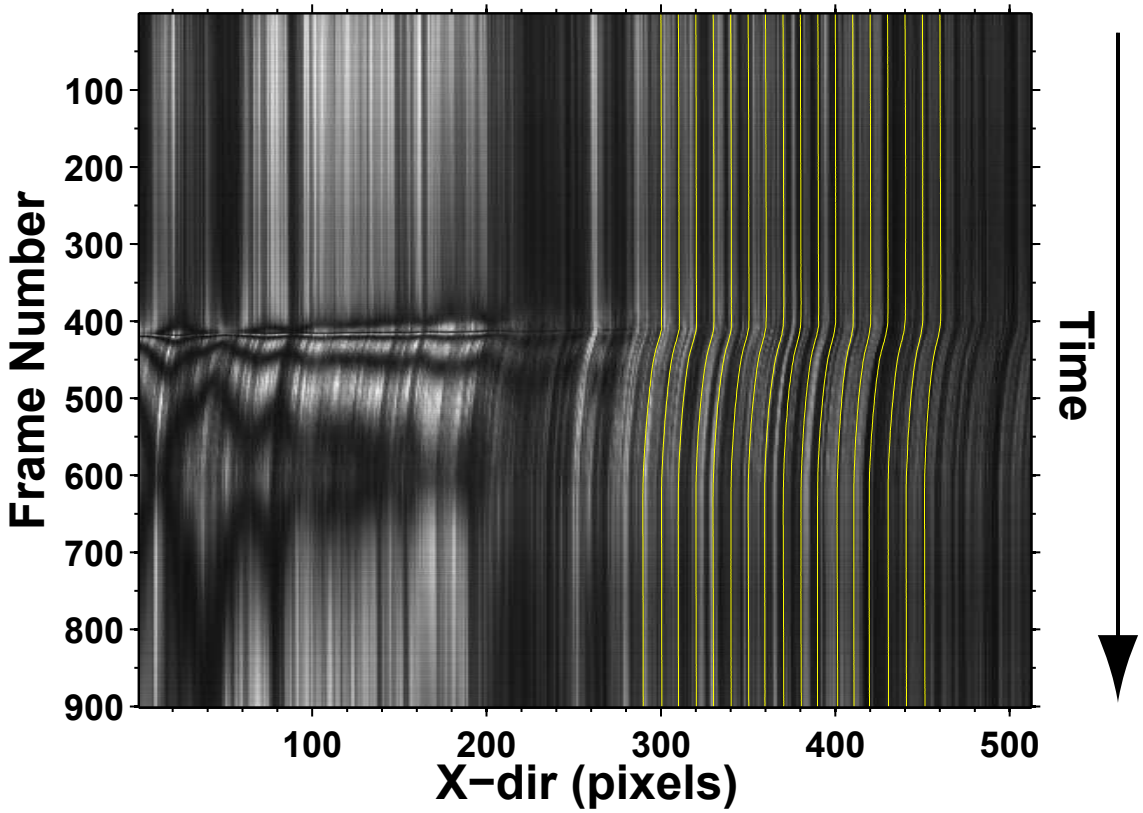

Figure 4.16: Image sequence for test case V3-P2, sliding velocity v_s= 2.2 mm/s and normal stress 0.22 MPa. Yellow traces are DIC tracked slip displacements.

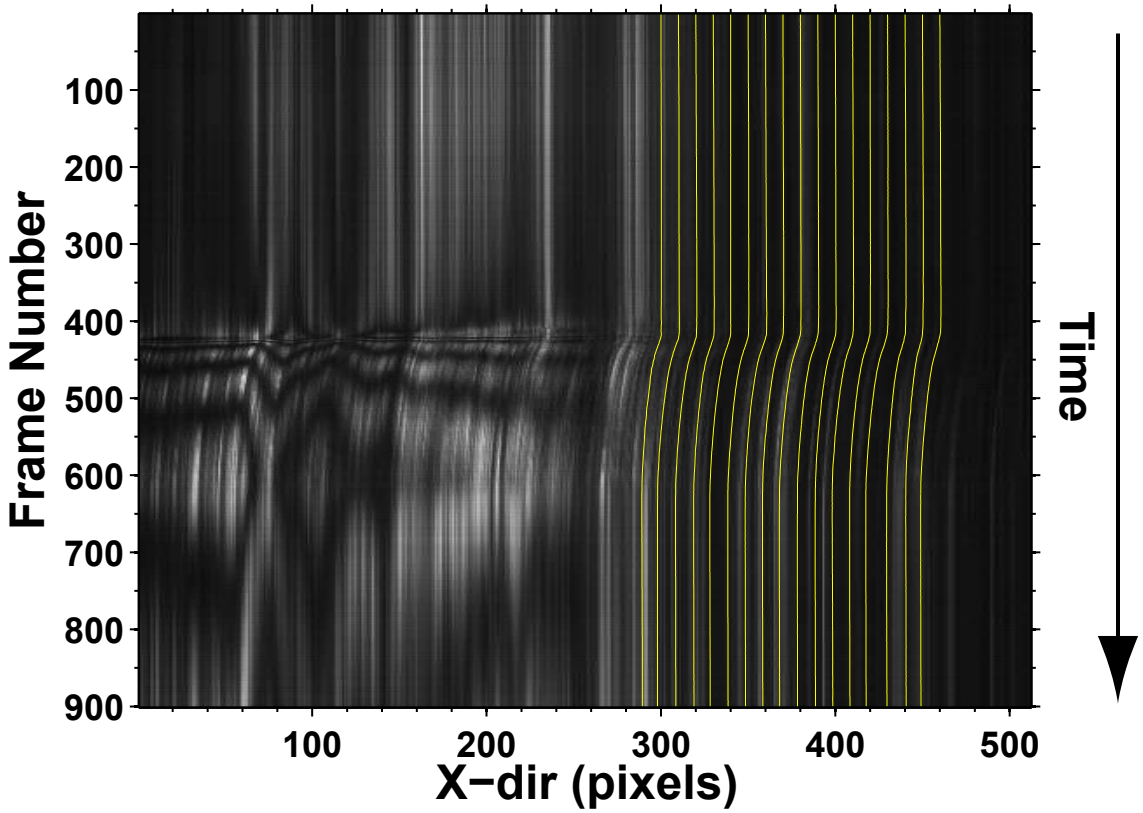

Figure 4.17: Image sequence for test case V3-P3, sliding velocity v_s= 2.2 mm/s and normal stress 0.30 MPa. Yellow traces are DIC tracked slip displacements.

4.5 Origin of Rupture Fronts

A critical problem in the study of slip onset is the origin of rupture. In fracture, the initial notch (pre-crack) is created based on the loading methodology to initiate fracture. In controlled friction experiments, slip can be initiated in a variety of loading configurations. The simplest and widely studied configuration is the one-dimensional block-slider configuration. A statically compressed material pair is sheared by constantly pushing one block at constant velocity. Slip can also be initiated by impacting a rigid projectile on one of the two blocks [23]. Another method of inducing slip is by compressing two blocks cut at an angle. Exploding wire sandwiched in the interface has also been used to induce slip [43]. Choosing frictional sliding configuration should be based on the problem being investigated. Earthquakes are frictional sliding in geo-scale where the origin of rupture is often discovered by inverting ground motion signatures collected at various seismic stations. The source of rupture influences the extent of damage and probability of the event repeating.

In this study, a simple one-dimensional block and slider configuration is used. The source of rupture from inversion of velocity data obtained from spatio-temporal plot prodicts the leading edge to be the origin of pulses. in order to confirm this, a series of experiments were performed on the sliding pair of PU-PMMA. Since, the direction of rupture waves were from leading to trailing edge, the focus was on the leading edge using photoelasticity. Framing rate of high speed camera was kept constant at

44,000 Hz as in previously reported experiments. Spatio-temporal plot constructed from a sequence of 78,000 images acquired over a duration of 1.6 seconds shows the evolution of fringes from the leading edge, as seen in Figure 4.18. The boundary conditions for this case are normal stress of 0.15 MPa and slider velocity of 1.5 mm/s. Two major slip events are marked by rupture fronts emitted from the leading edge at around Frame# 25000 and Frame# 68000. Zooming into the first slip event, as shown in Figure 4.19 demonstrates the origin of rupture waves at point 'O' close to the leading edge tip. Upon continuous shearing of interface, the leading edge is stretched until the elastic energy accumulated in the interface overcomes the frictional forces. At this point, rupture waves are emitted that accelerate towards the trailing edge at sub-shear speeds. The leading edge initiates the slip process which continues until the frictional forces overcome the slip, at which point the next stick phase begins. Weak ruptures were also observed intermittently, since their emission did not lead to slip. Such weak pulses lead to partial drop in shear stress close to the leading tip.

Analysis of photoelastic fringes for the stick-slip event was performed to determine the local value of μ at probe point P close to the sliding interface in PU sample. Figure 4.20 shows the variation in greyscale pixel value at probing point P as a function of time. Assuming a stress-free state after the onset of sliding during the first slip event, the periodic rise and fall of the greyscale levels were tracked to determine fringe order number. From slip#1 to slip#2, the fringe order number is found to be 2.5. The associated local friction coefficient prior to onset of second slip is estimated to be 1.4. The use of load sensors to measure normal and shear loads could yield only the nominal value of friction coefficient. But it is quite evident

from the results here clear that friction coefficient at any point along the interface is different during the onset of slip. We have successfully demonstrated a method of measuring local variations in shear stress using photoelasticity. By tracking the position of the leading edge tip, the amount of slip is estimated to be ≈0.30 mm.

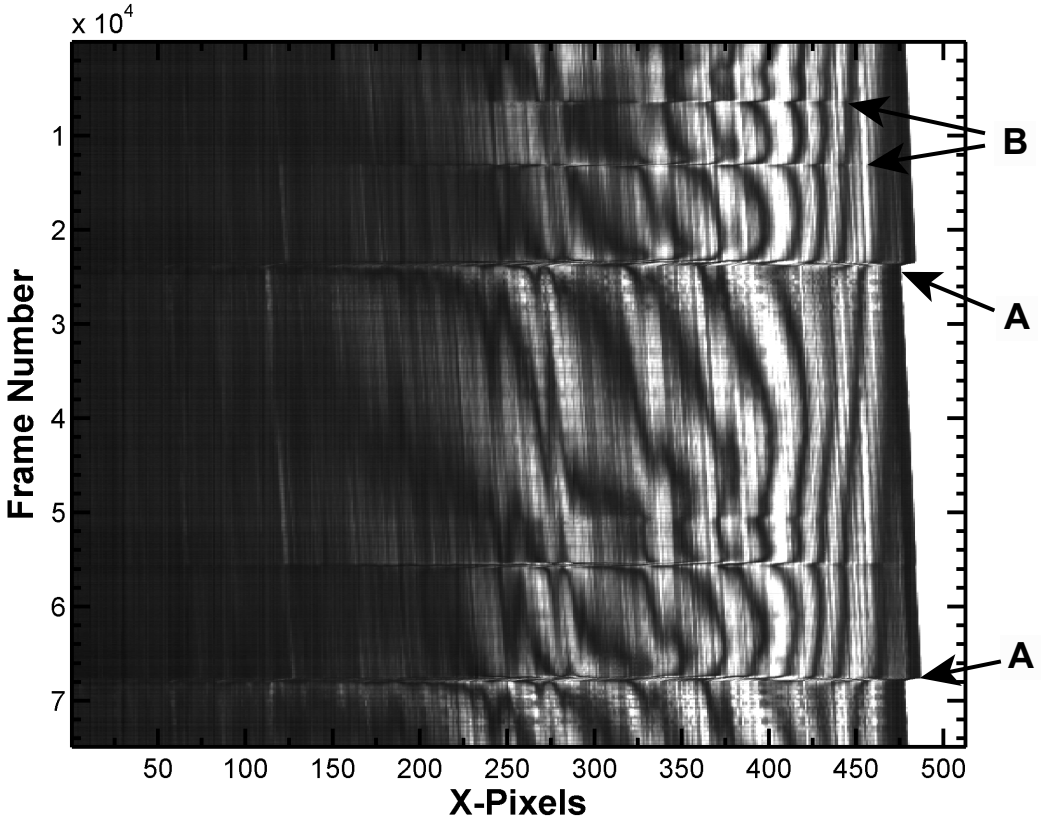

Figure 4.18: Spatio-temporal image sequence focusing on the leading edge of PU-PMMA sliding pair. Fringes represent contours of maximum shear stress in PU sample. The normal load is 0.15 MPa and slider velocity, v_s= 1.5 mm/s. Images were acquired at 44,000 frames per second. 'A' refer to the slip events, and 'B' refer to small-scale ruptures which produced no slip.

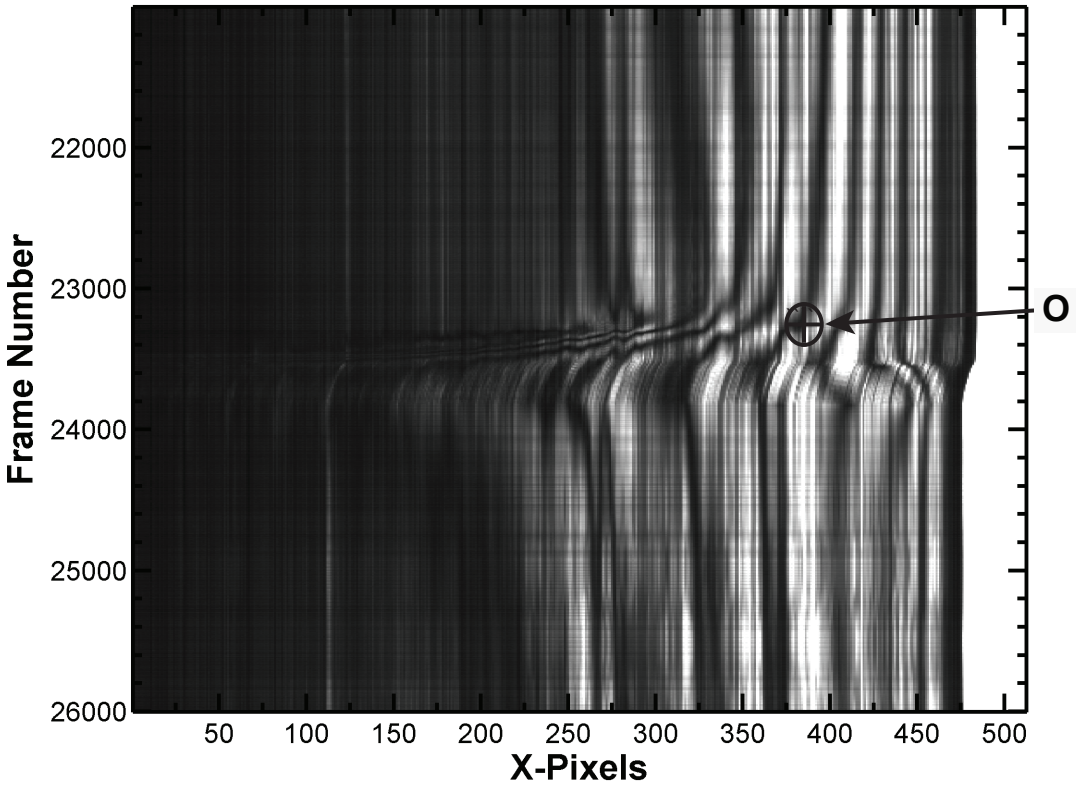

Figure 4.19: Spatio-temporal image sequence focusing on one slip event at the leading edge of PU-PMMA sliding pair. Fringes represent contours of maximum shear stress in PU sample. The normal load is 0.15 MPa and slider velocity, v_s= 1.5 mm/s. Images were acquired at 44,000 frames per second. By tracing the variation in fringe levels, the origin of ruptures can be narrowed down to a point indicated by 'O' in the figure. The magnitude of slip is about 0.30 mm.

4.6 Modified Origin of Rupture

In the previous section, the rupture nucleation point along homogeneous bimaterial interface of PU–PMMA was found to be at the leading edge. In order to investigate the effect of alternate rupture nucleation zones, a thin Teflon tape of 12.5 mm length was placed in the middle of the PU-PMMA interface, as seen in Figure 4.21. The

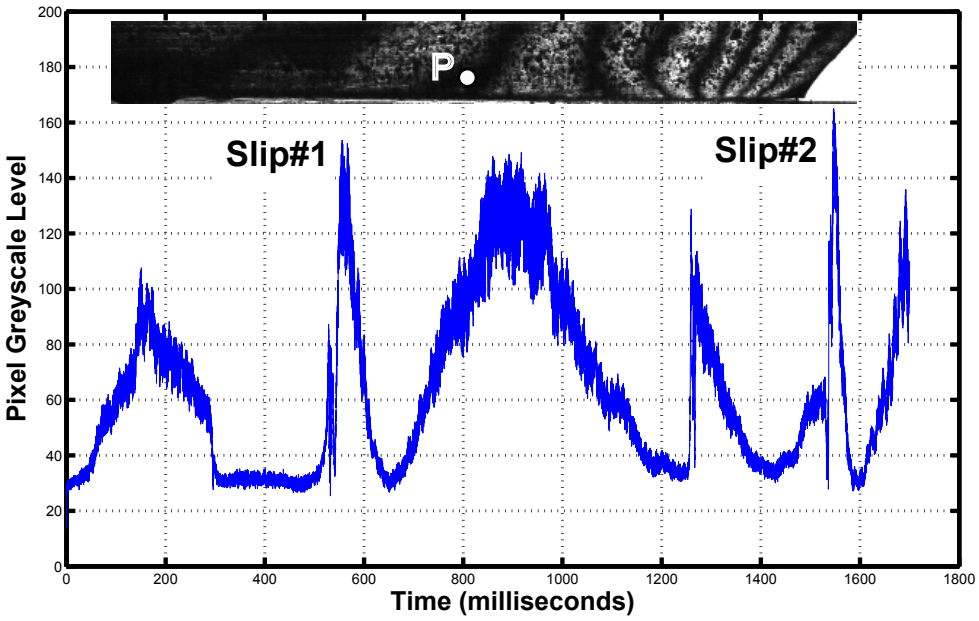

Figure 4.20: Plot of variation in greyscale pixel value at probing point P, close to the sliding interface, as a function of time. The interface is assumed to be free of shear at the slip#1. By tracking the periodic rise and fall of the greyscale levels, the fringe order number can be determined. From slip#1 to slip#2 the fringe order number is found to be 2.5. The local friction coefficient prior to the onset of second slip is estimated to be 1.4.

very low value of friction coefficient for Teflon-PMMA pair was expected provide the source of slip onset. Dynamic photoelasticity is used to observe the rupturing process via high speed camera framing at 44,000 frames per second. Such a system mimics a simple geometrical flat and uniform fault in earthquake terminology. Normal loading is kept constant using dead weights. The applied normal pressure was 0.15 MPa. The slider velocity was kept constant at 1.5 mm/s.

As the lower PMMA block is pushed at a constant rate, the top PU block undergoes shear strain due to the frictional locking of the two bodies at the interface.

Due to variability in the frictional resistance along the interface, particularly at low fault strength along the Teflon region, sudden loss of frictional strength could trigger rupture. Such triggering methodologies have been used previously in the numerical simulations by Ben-Zion and Andrews [11] and in experiments by Xia [43].

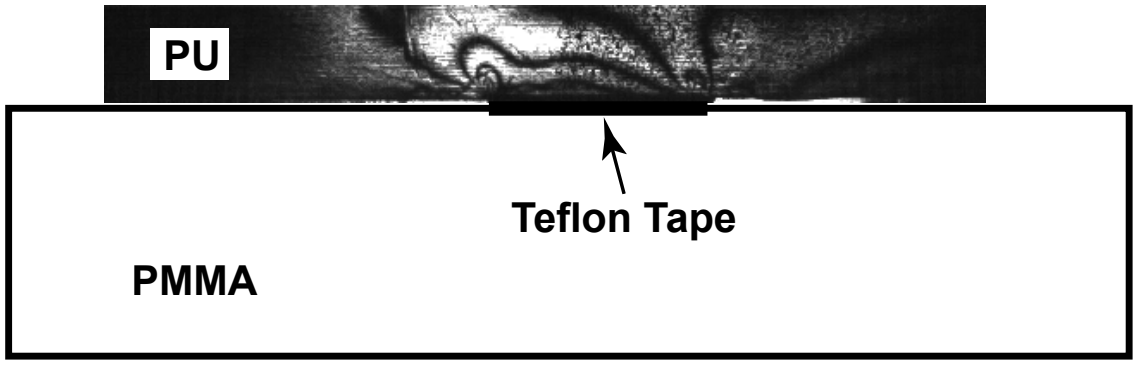

Figure 4.21: Schematic of a fault zone with weak nucleation point in the middle of the sliding interface. Weak frictional strength zone is introduced by sandwiching a thin Teflon film between PU-PMMA interface.

4.6.1 Experimental Observations

Spatio-temporal plots constructed from dynamic photoelastic images of PU-PMMA interface shows the progression of multiple stick-slip events, as seen in Figure 4.22. The repeated slip events occur at frequency of $\simeq$3 Hz. This is an increase from $\simeq$1 Hz for the case of PU-PMMA sliding pair with exactly same loading conditions. Detailed view of an isolated slip event is shown in Figure 4.23. As expected the rupture emission originated from the weak Teflon zone of the fault instead of the leading edge. Rupture waves can now propagate in two directions, (a) leading edge, and (b) trailing edge. Spatio-temporal plots show a strong wave propagation accelerating towards to the trailing edge. Weak waves originate from the fault zone

which head towards to the leading edge. High speed camera images show that slip in the leading edge begins only upon the arrival of the weak wavefronts. A third source of rupture waves originate from the leading edge as slip begins. DIC analysis of particle displacements show that the magnitude of slip was small, $\sim$0.05 mm. Maximum velocity of slip was also found to be around 25 mm/s. This shows that the presence of low strength fault zone acts as a trigger of premature ruptures. Weak zones in the faults increased the frequency of ruptures but decrease the magnitude, synonymous to small and frequent earthquakes. In the experiments conducted by Xia [43] where an rapidly expanding wire was used to source of rupture nucleation, similar bidirectional fronts were emitted at sub-shear speeds. In the case of dissimilar sliding pairs, propagation speeds were found to be directional in nature. The “preferred" direction was along the direction of slip in the softer material. Wrinkle-like Weertman pulses were observed during the sliding in his study. Earthquakes with preferential propagation direction have been reported too. In small earthquakes, ruptures propagating along the unfavorable direction were found to be arrested too. In the current study, sliding mode was continuous and crack-like in nature. No wrinkle-like pulses were detected. Due to the small field of view, the velocity of the rupture fronts could not be determined.

4.7 Estimation of Friction Coefficient from Photoelastic Fringe Analysis

One of the biggest challenges in friction is the determination of local friction coefficient at any point along the interface. Usually friction coefficient is measured at the global level using pressure or force sensors mounted in vertical and tangential

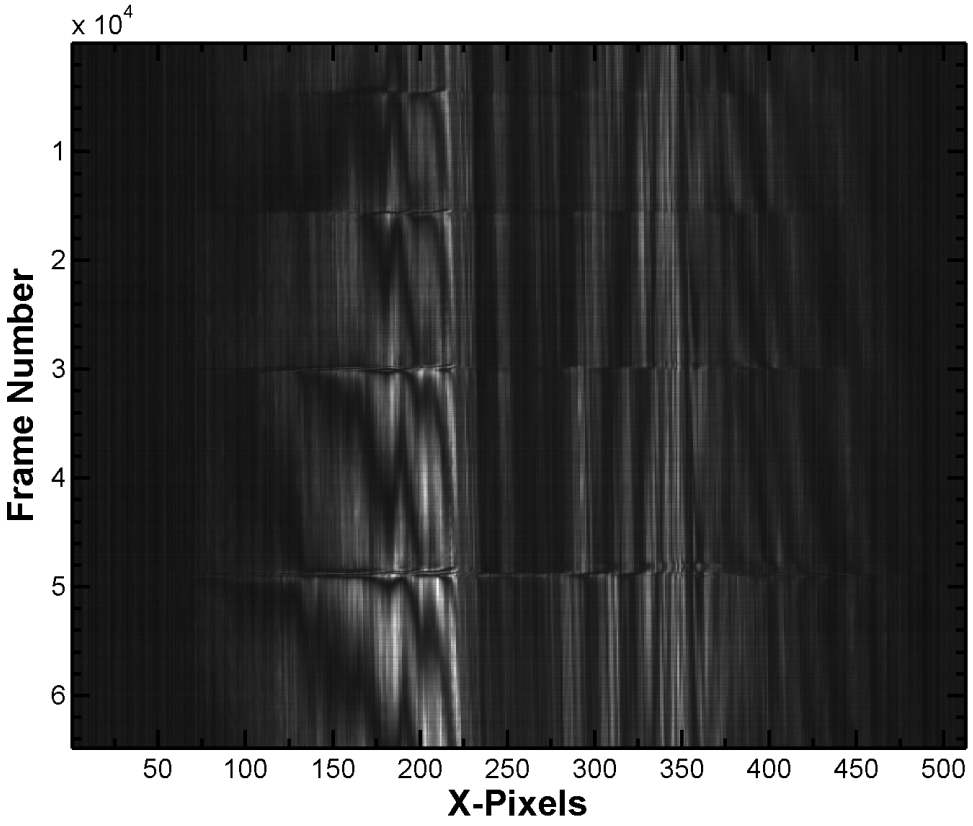

Figure 4.22: Spatio-temporal plot of dynamic photoelasticity fringes in PU specimen close to the sliding interface shows multiple stick-slip events. Weak frictional strength zone is in the center of field of view.

directions. The use of force sensors also introduces compliance and resolution issues and the resulting in averaged measurements. Such measurements are satisfactory if one is interested in studying the nominal friction behavior. However, in the case of seismic and tire-asphalt studies, localized values of friction coefficient is critical to identify the point of slip or rupture along the interface. The evolution of stress state during slip onset has remained elusive in developing a physical model for sliding.

In this study, we attempt to obtain the local value of friction coefficient using

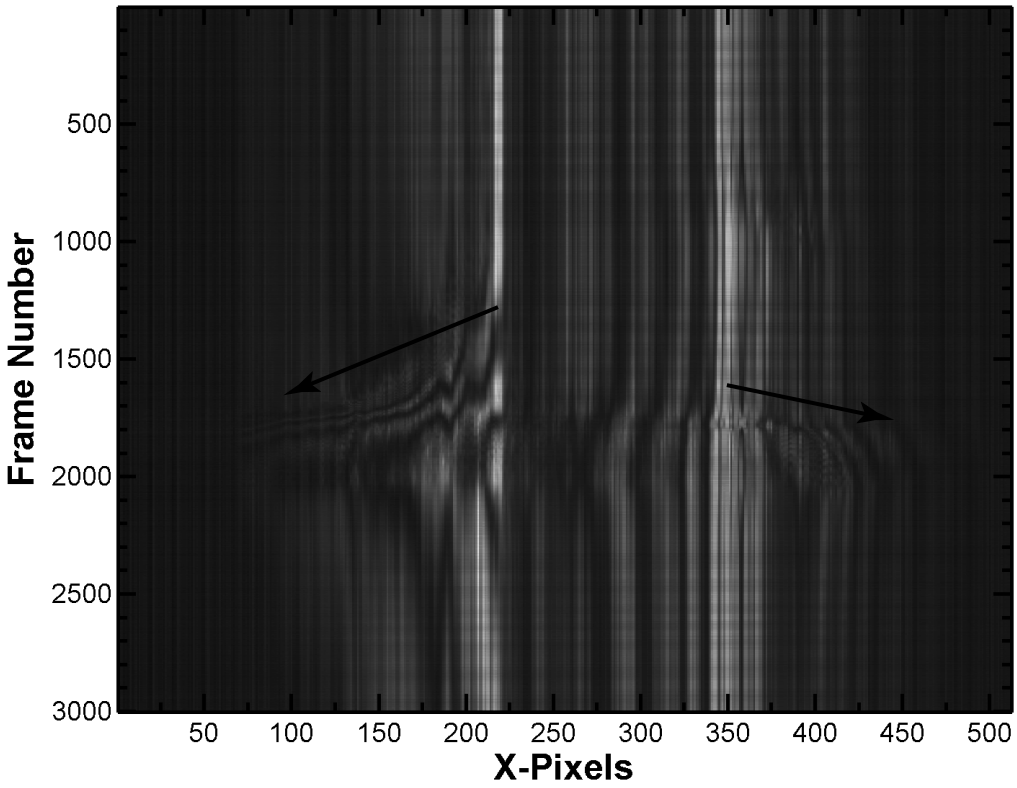

Figure 4.23: Spatio-temporal plot of dynamic photoelasticity fringes in PU specimen at an isolated stick-slip event. Weak frictional strength zone is in the center of field of view. Rupture propagation from this zone is found to propagate in two directions, strong rupture waves accelerating to the trailing edge, and weak waves propagating to the leading edge triggering the onset of slip there.

photoelastic fringes, which represent contours of maximum shear stress. By counting the passage of fringes at a point and assuming certain stress states, it is possible to determine the shear stress and hence the friction coefficient for a sliding pair. Using this approach, an expression for determining friction coefficient at a point was developed in Chapter 3 Section 3.2. Equation (3.4) was developed with the assumption that axial stresses are negligible at points away from leading and trailing

Table 4.4: Coefficient of friction (μ_{local}) determined from photoelastic fringe data for PU-PMMA interface and PU-Teflon-PMMA interface.

Test Case	Sliding Velocity (mm/s)	Normal Stress (MPa)	Fringe Number	μ_{local}
V2-P1	1.5	0.15	2.5	1.4
V2-P1 w/ Teflon	1.5	0.15	1	0.33

edges. Knowing the values of fringe constant, fringe number, and applied normal load, the value of friction coefficient can be estimated as follows:

$$\mu = \frac{1}{2}\sqrt{\frac{N^2 f_\sigma^2}{\sigma_y^2} - 1} \tag{4.1}$$

As stress waves propagate along the interface, the fringes levels change. To determine the fringe order number, a stress-free state is chosen. As documented earlier in this chapter, the stress levels along the interface drop to zero after the passage of the sub-shear waves. Fringe order numbers are counted from such a point in time and the friction coefficients are determined. The estimated friction coefficient represent the critical value at which slip occurs. Table 4.4 lists the values of μ_{local} calculated for PU-PMMA interface and PU-Teflon-PMMA interface.

CHAPTER 5

CONCLUSIONS

Real-time observations of onset of slip during frictional sliding in bimaterial interface of PU-PMMA were investigated. Two measurement techniques of dynamic photoelasticity and Digital Image Correlation were combined to simultaneously obtain wave and particle information during onset of sliding. Using a rigid load frame (rigid compared to the low elastic modulus of PU specimen), three different driving velocities and normal stresses were imposed. A high-speed camera with framing rate of 44,000 Hz was used to acquire images of stick-slip-stick sliding. From the photoelastic fringes, velocities of wave fronts were obtained. DIC analysis of the speckles on the surface of PU specimen provided slip magnitude, slip duration, and slip velocities. The findings in this study are summarized below:

- Prior to onset of slip, multiple wave fronts propagated through the interface in the direction opposite to tangential sliding of PMMA block, i.e. from leading to trailing edge. Friction coefficient was found to be dependent on the local stress state.

- The onset of sliding seemed to resemble shear crack-like mode. Magnitude of

slip was uniform at various points along the interface. Duration of slip at any point was equal to the total duration of the slip. However, a cascade of slow shear fronts propagating at similar speeds were observed. This is in contrast to single rupture front reported in literature. No detectable displacements in normal direction were found during slip onset, leading to conclusion that the process is governed by shear.

- Prior to onset of slip three distinct wave fronts were observed, (a) *Longitudinal wave* – small shear stress drop and no detectable slip, (b) *Shear wave* – drop in shear stress but no large scale slip, and (c) *Sub-shear waves* – drastic drop in shear stress across the interface and large scale slip initiates. Velocity of the slower sub-shear waves ranged from 30-80 m/s. No acceleration or bifurcation of the slow fronts were observed. Photoelastic fringes provided qualitative information on the maximum shear stress across the interface, hence no quantitative measure of shear stress was performed.

- Upon initiation of sliding, two distinct phases were identified: (a) *Acceleration phase* – velocity of slip increased and reached a peak value, indicating velocity-weakening friction regime, and (b) *Deceleration phase* – Velocity gradually dropped to zero indicating termination of slip phase. Contact rejuvenation by asperity pinning was observed from the gradual build-up of fringes across the interface. In all the test cases, duration of the acceleration phase was shorter than that of the deceleration phase. The ratio of acceleration phase duration to deceleration phase duration was found to be between 0.36 and 0.13.

- In the experiments conducted to investigate the role of driving velocity on

slip onset, three different velocities were used, namely, 0.5 mm/s, 1.5 mm/s, and 2.5 mm/s while the normal stress was maintained constantly at 0.15 MPa. Sliding velocity had a weak inverse effect on the slip magnitude while slip duration reduced with higher sliding speeds. Velocity of the sub-shear wave was found to increase from 30 m/s to 85 m/s when sliding velocities increased by about 4.5 times. Maximum velocity of slip was independent of sliding speed, ranging between 150–177 mm/s. With increase in sliding velocity, duration of acceleration phase decreased while the deceleration phase lasted longer with increase in driving velocity.

- Effects of normal stresses on slip onset and rupture wave fronts were investigated while keeping driving velocity constant. Three different normal stresses were chosen, namely, 0.15 MPa, 0.22 MPa, and 0.30 MPa. Due to the low elastic modulus and tensile strength of PU, the normal stresses were limited to 0.30 MPa. Sliding velocity was kept constant at 0.50 mm/s. Velocities of slow sub-shear fronts were found to be independent of normal load, ranging between 34 m/s and 46 m/s. Magnitude of slip nearly doubled when normal stresses increased by two times and maximum value of slip velocity also increased. While the overall duration of slip increased by $\sim$1.25 times, duration of acceleration phase was halved.

- The influence of normal stress was more pronounced than sliding velocity, on slip velocity, slip distance, and slip duration. Sliding velocity primarily influenced rupture wave speeds.

- Analysis of photoelastic fringes estimate the critical value of local friction

coefficient (μ_{local}) between 1.1. and 1.4, for different loading conditions.

- Origin of rupture was found to be close to the leading edge tip. Fluctuations in fringes prior to slip onset show rapidly accelerating rupture waves originating from a point on the interface close to the leading edge. Multiple wave propagation events were observed, however, not all of them resulted in a slip. Weak waves are accompanied by small drop in stress levels.

- Alternate fault zone was introduced in the middle of PU-PMMA sliding pair by sandwiching a thin Teflon tape between PU-PMMA interface. This narrow fault zone had relatively low friction coefficient. Dynamic photoelasticity images show shift in the rupture origination from leading edge to the fault zone. Wave ruptures from the fault zone propagated towards the leading and trailing edges. The ruptures propagating towards the trailing edge was stronger and faster. The weaker waves from fault zone triggered premature slip in leading edge of the PU sample. The stick-slip frequency increased and slip magnitude decreased. Introduction of the fault zone reduced the resistance of the interface to slip onset. Instantaneous slip velocities decreased by an order of magnitude from $\sim$200 mm/s to $\sim$20 mm/s.

The author hopes that the outcomes of this experimental study reported here will help guide the development/refinement of existing friction laws to better predict the onset of slip.

5.1 Further Work

The experiments clearly demonstrated the role of interface wave fronts and quantified the slips associated with their passage. Although, experiments were performed on bimaterial interface of PU on PMMA, we believe that similar results can be realized in other materials as well. We expect the trends observed in the sliding tests on PU–PMMA pair to be applicable to other materials as well. When rupture fronts span across different orders of velocities, it is critical to design the experiments such that all these events are captured. PU specimen could be replaced by PMMA or polycarbonate, where the wave speeds are much faster, in the order of 3000-6000 m/s. In order to do so, the acquisitions will have to be long enough. Previous studies of sliding onset by dynamic projectile impacts had high image acquisition rates but limited to very short durations. The fast p-wave and s-waves were captured but the slow sub-shear fronts were not acquired. Due to technological limitations on acquiring few hundred images at very fast framing rates of around 4000,000 to 800,000 Hz, it is difficult to observe similar slip patterns in materials with wave speeds close to that of earth's crust. Higher resolution of in-plane displacements can be obtained by interferometry techniques such as speckle pattern interferometry, however such techniques are sensitive to vibrations. Although, crack-like mode of sliding was observed in all the loading conditions, the measurements performed in this study lacked the resolution to capture such slip pulses.

Since frictional sliding shows a crack-like behavior, the next challenge lies in comparing frictional sliding and mode-II (pure shear) fracture. For the same material pair, comparison of stresses at onset of slip/failure can enable a fracture like

framework to describe frictional sliding.

BIBLIOGRAPHY

[1] A. Anooshehpoor and J.N. Brune. Frictional heat generation and seismic radiation in a foam rubber model of earthquakes. *PAGEOPH*, 142(3/4):735–747, 1994.

[2] A. Anooshehpoor and J.N. Brune. Wrinkle-like weertman pulse at the interface between two blocks of foam rubber with different velocities. *Geophysical Research Letters*, 26(13):2025–2028, 1999.

[3] M.C. Audry, C. Fretigny, A. Chateauminois, J. Teissere, and E. Barthe. Slip dynamics at a patterned rubber/glass interface during stick–slip motions. *The European Physical Journal E*, 35(9):1–7, 2012.

[4] M. Barquins and A.D. Roberts. Rubber friction variation with rate and temperature: Some new observations. *Journal of Physics D: Applied Physics*, 19(4):547, 1986.

[5] T. Baumberger and C. Caroli. Solid friction from stickŰslip down to pinning and aging. *Advances in Physics*, 55(3-4):279–348, 2006.

[6] T. Baumberger, C. Caroli, and O. Ronsin. Self-healing slip pulses along a gel/glass interface. *Physical Review Letters*, 88(7):075509, 2002.

[7] N.M. Beeler. Review of the physical basis of laboratory-derived relations for brittle failure and their implications for earthquake occurrence and earthquake nucleation. *Pure and Applied Geophysics*, 161:1853 – 1876, 2004.

[8] N.M. Beeler and T.E. Tullis. Self-healing slip pulses in dynamic rupture models due to velocity-dependent strength. *Bulletin of the Seismological Society of America*, 86(4):1130–1148, 1996.

[9] O. Ben-David, G. Cohen, and J. Fineberg. The dynamics of the onset of frictional slip. *Science*, 330(6001):211–214, 2010.

[10] O. Ben-David and J. Fineberg. Static friction coefficient is not a material constant. *Physical Review Letters*, 106:254301, 2011.

[11] Y. Ben-Zion and D.J. Andrews. Properties and implications of dynamic rupture alogn a material interface. *Bulletin of the Seismological Society of America*, 88(4):1085–1094, 1998.

[12] P. Berthoud, T. Baumberger, C. G'Sell, and J.-M. Hiver. Physical analysis of the state- and rate-dependent friction law: Static friction. *Physical Review B*, 59:14313–14327, 1999.

[13] F.P. Bowden and D. Tabor. *The Friction and Lubrication of Solids I*. Clarendon Press, London, 1950.

[14] W.F. Brace and J.D. Byerlee. Stick-slip as a mechanism for earthquakes. *Science*, 153(3739):990–992, 1966.

[15] J.D. Byerlee. The mechanics of stick-slip. *Tectonophysics*, 9:475–486, 1970.

[16] D. Coker, G. Lykotrafitis, A. Needleman, and A.J. Rosakis. Frictional sliding modes along an interface between identical elastic plates subject to shear impact loading. *Journal of The Mechanics and Physics of Solids*, 53:884–922, 2005.

[17] J.H. Dieterich. Time-Dependent Friction in Rocks. *Journal of Geophysical Research*, 77:3690–3697, 1972.

[18] J.H. Dieterich. Modeling of rock friction 1. Experimental results and constitutive equations. *Journal of Geophysical Research*, 84:2161–2168, 1979.

[19] J.H. Dieterich and B.D. Kilgore. Direct observation of frictional contacts: New insights for state-dependent properties. *Pure and Applied Geophysics*, 143:283–302, March 1994.

[20] Y. Fukahori, P. Gabriel, and J.J.C. Busfield. How does rubber truly slide between schallamach waves and stickŰslip motion? *Wear*, 269:854–866, 2010.

[21] T.H. Heaton. Evidence for and implications of self-healing pulses of slip in earthquake rupture. *Physics of the Earth and Planetary Interiors*, 64(1):1–20, 1990.

[22] H. Lu and P.D. Cary. Deformation measurements by digital image correlation: Implementation of a second-order displacement gradient. *Experimental Mechanics*, 40(4):393–400, 2000.

[23] Lykotrafitis. *Experimental Study of Dynamic Frictional Sliding modes along incoherent interfaces*. PhD thesis, California Institute of Technology, 2006.

[24] G. Lykotrafitis and A.J. Rosakis. Dynamic sliding of frictionally held bimaterial interfaces subjected to impact shear loading. *Proceedings of the Royal Society A*, 462(2074):2997–3026, 2006.

[25] C. Marone. Laboratory-derived friction laws and their application to seismic faulting. *Annual Review of Earth and Planetary Sciences*, 26(1):643–696, 1998.

[26] X.D. Pan. *Recent Advances in Rubber Friction in the Context of Tire Traction*, chapter 11, pages 443–499. John Wiley & Sons, Inc., 2013.

[27] B.N.J. Persson. Rubber friction and tire dynamics. *Journal of Physics: Condensed Matter*, 23(1):015003, 2011.

[28] B.N.J. Persson, O. Albohr, U. Tartaglino, A.I. Volokitin, and E. Tosatti. On the nature of surface roughness with application to contact mechanics, sealing, rubber friction and adhesion. *Journal of Physics: Condensed Matter*, 17(1):R1, 2005.

[29] E. Rabinowicz. The intrinsic variables affecting the stick-slip process. *Proceedings of the Physical Society*, 71(4):668, 1958.

[30] E. Rabinowicz. Frictio coefficients of noble metals over a range of loads. *Wear*, 152:89–94, 1992.

[31] J.R. Rice and A.L. Ruina. Stability of steady frictional slipping. *Journal of Applied Mechanics*, 50:343–349, 1983.

[32] S.M. Rubinstein, G. Cohen, and J. Fineberg. Detachment fronts and the onset of dynamic friction. *Nature*, 430:1005–1009, 2004.

[33] S.M. Rubinstein, G. Cohen, and J. Fineberg. Contact area measurements reveal loading-history dependence of static friction. *Physical Review Letters*, 96:256103, Jun 2006.

[34] S.M. Rubinstein, G. Cohen, and J. Fineberg. Cracklike processes within frictional motion: Is slow frictional sliding really a slow process? *MRS Bulletin*, 33:1181–1189, 2008.

[35] S.M. Rubinstein, G. Cohen, and J. Fineberg. Visualizing stickŰslip: experimental observations of processes governing the nucleation of frictional sliding. *Journal of Physics D: Applied Physics*, 42(21):214016, 2009.

[36] A. Ruina. Slip instability and state variable friction laws. *Journal of Geophysical Research*, 88(B12):10359–10379, 1983.

[37] A. Schallamach. The load dependence of rubber friction. *Proceedings of the Physical Society. Section B*, 65(9):657, 1952.

[38] M.A. Sutton, W.J. Walters, W.H. Peters, W. F. Ranson, , and S.R. McNeil. Determination of displacement using an improved digital correlation method. *Image and Vision Computing*, 1(3):133–139, 1983.

[39] K.H. Tsai and K.S. Kim. The micromechanics of fiber pull-out. *Journal of the Mechanics and Physics of Solids*, 44(7):1147–1177, 1996.

[40] A. Vanossi, N. Manini, M. Urbakh, S. Zapperi, and E. Tosatti. Modeling friction: from nano to meso scales. *ArXiv e-prints: http://arxiv.org/abs/1112.3234*, 2012.

[41] J. Weertman. Dislocations moving uniformly on the interface between isotropic media of different elastic properties. *Journal of Mechanics and Physics of Solids*, 11:197–204, 1963.

[42] J. Weertman. Unstable slippage across a fault that separates elastic media of different elastic constants. *Journal of Geophysical Research: Solid Earth*, 85(B3):1455–1461, 1980.

[43] K. Xia. *Laboratory Investigations of Earthquake Dynamics*. PhD thesis, California Institute of Technology, 2005.

[44] G. Zheng and James R. Rice. Conditions under which velocity-weakening friction allows a self-healing versus a cracklike mode of rupture. *Bulletin of the Seismological Society of America*, 88(6):1466–1483, 1998.

VITA

Vijay Krishnan Subramanian

Candidate for the Degree of

Doctor of Philosophy

Thesis: MECHANISMS GOVERNING ONSET OF SLIDING FRICTION

Major Field: Mechanical Engineering

Biographical:

Personal Data: Born in Chennai, Tamil Nadu, India on November 21, 1982, the son of K. Subramanian and Uma Subramanian.

Education: Received the Bachelor of Engineering (B.E.) degree in Mechanical Engineering from Anna University, Chennai, Tamil Nadu, India, in May 2005. Received the Master of Science in degree in Mechanical Engineering from Oklahoma State Univeristy, Stillwater, Oklahoma, U.S.A. in August 2010. Completed the requirements for the degree of Doctor of Philosophy degree with a Major in Mechanical Engineering at Oklahoma State University, Stillwater, Oklahoma, U.S.A., in July, 2014.